gene. NIH3T3 cells are a well-established fibroblast cell line, so that it is easy to optimize conditions for gene transfer and to select gene-expressing cells *in vitro*. In addition, fibroblasts are available from various human sources, which may be advantage for extending future clinical investigations. We transfected NIH3T3 cells with the *Bdnf* gene using lipofection. We then examined the potential for transplanting transfected NIH3T3 cells into the mouse inner ear.

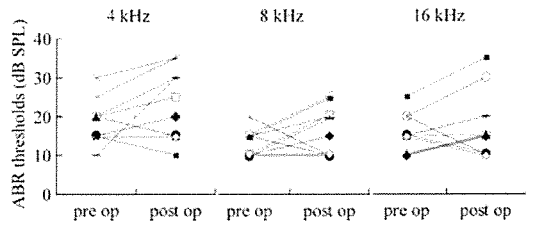

FIG. 1. ABR thresholds before and after cell transplantation. The left lane shows preoperative (pre op) ABR thresholds of each ear, and the right shows those recorded on day 28 after transplantation (post op) at 4, 8, and 16 kHz. The *x* axis shows ABR thresholds (dB SPL).

Results and Discussion

Bdnf Gene Transfer

To determine the efficacy of gene transfection using a nonviral vector, we performed reverse transcriptase-polymerase chain reaction (RT-PCR) analysis of Bdnf mRNA levels in transfected and nontransfected NIH3T3 cells (data not shown). NIH3T3 cells transfected with the mouse *Bdnf* gene (NIH3T3/BDNF) demonstrated Bdnf mRNA expression (86-bp fragment), which was absent from cells transfected with a vector carrying an antibiotic resistance gene (NIH3T3/control) and from nontransfected cells (NIH3T3/original). Amplification of gylceraldehyde-3-phosphate dehydrogenase (*Gapdh*), yielding a 171-bp amplicon, was used as an internal control. Negative control reactions that lacked reverse transcriptase failed to yield amplicons of either *Gapdh* or *Bdnf*.

We carried out an enzyme-linked immunosorbent assay (ELISA) for Bdnf protein to examine the efficacy of Bdnf protein expression and secretion *in vitro*. The mean Bdnf concentration in the culture medium of NIH3T3/BDNF cells, at 396.70 ± 32.66 pg/ml, was significantly higher than in the medium of either NIH3T3/control cells (24.96 ± 5.22 pg/ml) or NIH3T3/original cells (32.42 ± 7.09 pg/ml) ($P < 0.0001$). These findings demonstrate efficient, functional gene transfer into NIH3T3 cells *in vitro* by a liposome-mediated delivery method.

Cell Transplantation into Mouse Cochleae

We transfected NIH3T3 cells with the mouse *Bdnf* gene tagged with a FLAG epitope (NIH3T3/FLAG) to enable transfected, transplanted cells to be readily distinguished from host inner ear cells. We injected suspensions of NIH3T3/FLAG and NIH3T3/control cells into the perilymphatic space of the posterior semicircular canal of C57BL/6 mice using a technique that we developed in previous studies [17,18]. Although delivery of cells into the mouse cochlea is difficult because of its small size, the well-defined genetics of a mouse model enable a variety of analyses of the inner ear to be performed.

We performed auditory brain stem response (ABR) recording to evaluate the effects of the transplantation procedure on hearing (Fig. 1). Alterations in ABR thresholds between pre- and postoperation were limited within 10 dB, although one animal exhibited a 20-dB elevation in ABR thresholds at 4 kHz. Preoperative ABR thresholds were 18.6 ± 1.7 (dB SPL) at 4 kHz, 12.7 ± 1.0 at 8 kHz, and 15.5 ± 1.4 at 16 kHz, and those on postoperative day 28 were 22.7 ± 2.6 at 4 kHz, 15.9 ± 1.9 at 8 kHz, and 17.3 ± 2.5 at 16 kHz. We identified no significant elevation of ABR thresholds on day 28 at frequencies of 4, 8, and 16 kHz. In addition, we observed no vestibular dysfunction in the behavior of the animals after the operation. These findings indicate the limited surgical invasiveness of our transplantation procedure, which is almost identical to previous observations [19,20].

Immunohistochemical analysis of FLAG expression demonstrated the settlement and survival of grafted NIH3T3/FLAG cells in both the cochlea and the vestibule (Figs. 2A, 2B, 2D, 2E). The engrafted cells were clearly distinct from the endogenous cells based on their expression of FLAG, while control specimens that were transplanted with NIH3T3/control cells exhibited no expression of FLAG (Figs. 2C and 2F). Grafted cells were localized in the perilymphatic space of cochleae or vestibules and did not establish in the endolymphatic space or within the inner ear tissues. These locations are identical to those of neural stem cell-derived cells transplanted into the mouse inner ear through the semicircular canal in our previous study [17]. On day 7, we found numerous grafted cells as cell aggregates in the vestibule. On day 28, we still observed grafted cells in both vestibules and cochleae, but did not see aggregation of grafted cells. Of grafted cells located in the perilymphatic space of cochleae, 91.2 ± 11.1% adhered to host cochlear tissues on day 7 and 92.3 ± 14.7% on day 28. The survival and settlement of grafted cells in the inner ear were also demonstrated by Western blotting for FLAG (Fig. 2G). We prepared protein lysates from the inner ear specimens obtained on day 28. The FLAG-tagged *Bdnf* transgene product (31 kDa) was detected in specimens transplanted with NIH3T3/FLAG cells, but not in those transplanted with NIH3T3/control cells. The β-actin internal control was detected in both specimens at equal density. These findings demonstrate that cells transplanted through the posterior semicircular canal survive and produce gene-encoded proteins in the perilymphatic space of cochleae and vestibules, indicating

Copyright © The American Society of Gene Therapy

doi:10.1016/j.ymthe.2006.06.012

FIG. 2. Localization of grafted NIH3T3/FLAG cells in the inner ear and infiltration of CD45-positive cells in cochleae. (A–F) Grafted cells are labeled with FLAG (green fluorescence), and cell nuclei are labeled with DAPI (blue fluorescence). A number of grafted cells are found both in the cochlea (A) and in the vestibule (D) at 1 week after transplantation. In the vestibule, numerous grafted cells form cell aggregates (D). Grafted cells are also identified in the cochlea (B) and vestibule (E) at 4 weeks after transplantation. No FLAG-positive cells were found in the control cochlea (C) or vestibule (F). Bars represent 200 μm and 20 μm in insets. (G) Western blot for FLAG expression in the inner ear at 4 weeks after cell transplantation. The FLAG-tagged Bdnf (31-kDa band) is detected in cochleae engrafted with NIH3T3/BDNF-FLAG cells (lane 1), but not in engrafted control cells (lane 2). β-Actin (42-kDa band), an internal control, is detected in both specimens at the same density. (H–J) Localization of CD45-positive cells in cochleae. In control cochleae, CD45-positive cells (red fluorescence) are found in the spiral ligament and spiral ganglion (arrows in H). CD45-positive cells were localized in the spiral ganglion, osseous spiral lamina, spiral ligament, and spiral limbus (arrows) at 1 (I) and 4 weeks (J) after engraftment of NIH3T3/BDNF-FLAG cells. Blue fluorescence shows DAPI. Bars represent 200 μm.

Copyright © The American Society of Gene Therapy

sustained delivery of Bdnf from transplanted cells to the perilymphatic space of the inner ears. Previous investigations have demonstrated that application of neurotrophins, including Bdnf, into the perilymph efficiently protects hair cells or spiral ganglion neurons from various ototoxic insults [2–6,10,11], indicating that neurotrophins delivered in the perilymph act on hair cells and spiral ganglion neurons. We therefore consider that Bdnf secreted from transplanted cells may be accessible to hair cells and spiral ganglion neurons.

The numbers of FLAG-positive cells in the cochlea decreased from the time point of day 7 to that of day 28. On day 7 after transplantation, we observed 26.7 ± 3.3 grafted cells in one midmodiolus section of cochleae, while we found 14.4 ± 2.3 cells on day 28. We then analyzed infiltration of inflammatory cells into cochlear tissues to investigate immune-mediated clearance of grafted cells. We employed immunohistochemistry for CD45, a leukocyte common antigen, to determine the distribution of inflammatory cells in the cochlea. In control cochleae, we found CD45-positive cells in the spiral ganglion, spiral limbus, and spiral ligament (Fig. 2H). Cochleae that received transplantation of NIH3T3/FLAG cells exhibited a similar distribution of CD45-positive cells compared to that of control cochleae (Figs. 2I and 2J). We observed no obvious infiltration of CD45-positive cells into the perilymphatic space of cochleae. These findings demonstrate that infiltration of inflammatory cells is not induced by transplantation of NIH3T3/FLAG cells into the inner ears. Even after xenografts into the cochlear fluid space without use of immune suppressants, cell infiltration into the cochlear fluid space has not been observed [21]. We therefore consider that immune-mediated clearance may not play a central role in elimination of transplanted cells from the inner ear. However, further studies are required to determine actual roles of the immune system in the decrease in transplanted cells in the inner ears.

Efficiency of Gene Delivery

We performed an ELISA of Bdnf proteins extracted from the inner ear to examine the efficiency of cell–gene delivery. We collected the inner ear specimens on day 7 after transplantation and calculated the ratio of Bdnf concentration to total protein in the sample solutions. NIH3T3/BDNF cell-transplanted specimens showed a significantly higher ratio (93.40 ± 10.69 pg/mg total protein) compared with NIH3T3/control cell-transplanted samples (46.68 ± 4.41 pg/mg) ($P = 0.01$). There was no significant difference between the levels of total protein extracted from the two samples (NIH3T3/BDNF, 2.65 ± 0.21 mg/ml; NIH3T3/control, 2.77 ± 0.12 mg/ml). These findings demonstrate that Bdnf synthesis by engrafted NIH3T3/BDNF cells contributes to a significant increase in Bdnf protein levels of the inner ear specimens, suggesting that cell–gene therapy may be applicable for local, sustained delivery of therapeutic molecules into the inner ear.

This is the first report that demonstrates the successful cell–gene delivery of therapeutic molecules to the cochlea without the use of viral vectors, an encouraging result for the extension of research into gene therapy for the inner ear. Currently, several experiments utilize human fibroblasts as a delivery vehicle [22,23]. The use of autologous bone marrow-derived stromal cells for transplants into the inner ear has been reported [24]. Such cells eliminate the risk of immunoresponses, and their ability to migrate into the cochlear lateral wall and modiolus is likely to enhance the potential for delivery of genes into these areas of the cochlea. Future studies should be performed to evaluate the potential of these alternative transplant media as a vehicle for gene delivery.

In summary, we transplanted NIH3T3 cells that had been genetically engineered to express Bdnf into the mouse inner ear and evaluated the efficiency of transplantation for local delivery of gene products. The results demonstrated a significant increase in Bdnf protein in the inner ear following transplantation of engineered cells. These findings indicate that gene therapy may be a feasible treatment option for inner ear diseases such as SNHL. Cell–gene delivery of therapeutic molecules into the inner ear is suitable for protection of inner ear cells against gradually progressive degeneration. Presbycusis, age-related hearing loss, may be included in targets for cell–gene therapy. BDNF application via cell–gene delivery could be an efficient strategy for promotion of survival of SGNs in cases of cochlear implants (CIs), which are small devices that are surgically implanted in the cochlea to stimulate SGNs. BDNF transgene produced by gene-engineered cells will support the survival of SGNs after CI surgery, which can contribute to the maintenance of hearing benefits provided by CIs.

Materials and Methods

Animals. Forty-three 10-week-old male C57BL/6 mice (SLC Japan, Hamamatsu, Japan) with normal hearing were used in the study. All mice were maintained in the Institute of Laboratory Animals, Kyoto University Graduate School of Medicine. All experimental protocols were approved by the Animal Research Committee, Kyoto University Graduate School of Medicine, and conducted in accordance with NIH guidelines for the care and use of laboratory animals.

Vector construction. The *Mus musculus* (house mouse) brain-derived neurotrophic factor cDNA clone (GenBank Accession No. BC034862) was obtained from Invitrogen (Carlsbad, CA, USA). PCR amplification of the cDNA using Pyrobest DNA polymerase (TaKaRa-Bio, Kyoto, Japan) was performed with the following primer pairs: 5′ primer, 5′-GGAATTCGCCACCATGACCATCCTTTTCCTTACTATGG-3′; 3′ primer 1, 5′-ATAAGAATAAGCGGCCGCTCATCTTCCCCTTTTAATGGTCAGTG-3′; and 3′ primer 2, incorporating two pairs of FLAG epitope, 5′-ATAAGAATAAGCGGCCGCTCACTTGTCATCGTCGTCCTTGTAGTCCTTGTCATCGTCGTCCTTGTAGTCCTTGTCATCGTCGTCCTTGTAGTCTCTTCCCCTTTTAATGGTCAGTG-3′. PCR products were digested with *Eco*RI and *Not*I, and a 0.77-kb

Copyright © The American Society of Gene Therapy

doi:10.1016/j.ymthe.2006.06.012

*Eco*RI–*Not*I fragment containing mouse *Bdnf* or mouse *Bdnf* with FLAG epitope was cloned into the *Eco*RI–*Not*I site of the pIRESneo3 vector (BD Biosciences, Palo Alto, CA, USA) using Ligation Solution (TaKaRa-Bio) to generate plasmid pIRESneo3-bdnf (supplementary information) or pIRESneo3-bdnfflag. For subsequent experiments, plasmid pIRESneo3 containing the neomycin-resistant gene only (pIRESneo3-control) was also amplified. Restriction analysis and DNA sequencing were used to confirm the integrity of all constructs.

Cell lines and gene transfer. NIH3T3 cells were obtained from Riken Cell Bank (RCB 0150; Tsukuba, Japan) and cultured in Dulbecco's modified Eagle's medium (DMEM; GIBCO BRL, Grand Island, NY, USA) containing 10% newborn calf serum (GIBCO), penicillin (100 U/ml), streptomycin (100 μg/ml), and amphotericin B (0.25 μg/ml) in a humidified atmosphere of 5% CO_2 at 37°C. NIH3T3 cells were plated at a density of 1×10^5 cells per 100-mm plastic dish and incubated for 48 h. Transfection was performed with 18 μl of FuGENE6 Transfection Reagent (Roche, Indianapolis, IN, USA) complexed with 9 μg pIRESneo3-bdnf, pIRESneo3-bdnfflag, or pIRESneo3-control plasmid in DMEM per 100-mm plastic dish at 37°C for 6 h. The medium was then replaced with conditioned medium containing Geneticin sulfate (G418; Sigma, St. Louis, MO, USA) for the selection of stably transfected cell clones.

Bdnf mRNA expression in cell lines. The expression of Bdnf mRNA in the cell lines was analyzed with RT-PCR. Total RNA was extracted from the cultured cell lines using the RNeasy Kit (Qiagen GmbH, Germany) and then treated with DNase I (Ambion, Austin, TX, USA). Four sets of total RNA for each cell line were prepared. PCRs were performed using TaqMan Gold PCR Master Mix (Applied Biosystems, Foster City, CA, USA) and Bdnf-specific primers. Gapdh mRNA was used as the invariant control. All reactions were performed in triplicate.

Bdnf secretion from cell lines. Bdnf protein levels in culture medium were measured by ELISA to examine Bdnf secretion by transfected cells. NIH3T3/BDNF, NIH3T3/control, and NIH3T3/original cells (1×10^5) were inoculated in 60-mm plastic dishes with 3 ml conditioned medium. The supernatants of the conditioned media were harvested approximately 24 h after inoculation. ELISA was performed using the BDNF Emax Immunoassay System (Promega, Madison, WI, USA) according to the manufacturer's instructions. Four sets of samples were prepared from each cell line, and all reactions were performed in triplicate.

Cell transplantation. On the day of transplantation, cultured cells were suspended at 3×10^4 cells/μl DMEM/F12 (GIBCO). NIH3T3/BDNF cells were transplanted into 10 animals, NIH3T3/FLAG cells into 24 animals, and NIH3T3/control cells into 9 animals. Cell transplantation was performed under general anesthesia with 75 mg/kg ketamine and 9 mg/kg xylazine. A retroauricular incision was made in the left ear, and the posterior semicircular canal (PSCC) was exposed. A small hole was made in the bony wall of the PSCC. A fused silica glass needle (EiCOM, Kyoto, Japan) was then inserted into the perilymphatic space of the PSCC, and the cell suspension was injected at the rate of 1 μl/min for 3 min using a Micro Syringe Pump (EiCOM).

Measurement of auditory function. The auditory function of experimental animals was monitored by ABR recording. ABR measurements were performed as previously described [25]. ABRs were recorded before cell transplantation and on day 28 in the 11 animals that received an engraftment of NIH3T3/FLAG cells. Thresholds were determined for frequencies of 4, 8, and 16 kHz.

Immunohistochemistry. Under general anesthesia, the animals that had been engrafted with NIH3T3/BDNF-FLAG cells were transcardially perfused with phosphate-buffered saline, pH 7.4, followed by 4% paraformaldehyde in phosphate buffer at pH 7.4 on day 7 ($n=10$) or 28 ($n=10$). Immediately, the temporal bones were dissected out and immersed in the same fixative for 4 h at 4°C. Specimens were prepared as cryostat sections. Two midmodiolus sections were chosen from each specimen and stained by immunohistochemistry for FLAG to distinguish transplanted cells from host specimens. Two cochleae on day 7 after transplantation of NIH3T3/control cells were used as controls for immunostaining for FLAG. We counted the numbers of FLAG-positive cells and those of FLAG-positive cells that adhered to cochlear tissues. The ratios of grafted cell that adhered to cochlear tissues were then calculated. The emergence of CD45-positive cells was also examined to evaluate inflammatory response following cell transplantation. Untreated cochlear specimens were served as controls for immunostaining for CD45. Anti-FLAG M2 mouse monoclonal antibody (1:230; Sigma) or anti-mouse CD45 rat monoclonal antibody (a leukocyte common antigen, Ly-5, 1:20; BD PharMingen, San Diego, CA, USA) was used as the primary antibody, and FITC-conjugated goat anti-mouse antibody (1:500; Santa Cruz Biotechnology, Santa Cruz, CA, USA) or Alexa-Fluor 546-conjugated anti-rat antibody (1:500; Molecular Probes, Eugene, OR, USA) was used as the secondary antibody. Counterstaining by 4′,6-diamidino 2-phenylindole dihydrochloride (DAPI; 1 μg/ml; Molecular Probes) was performed to demonstrate nuclear locations.

FLAG Western blotting. The expression of FLAG-tagged Bdnf fusion protein in the inner ear engrafted with NIH3T3/FLAG cells ($n=4$) or NIH3T3/control cells ($n=4$) was determined by Western blotting 28 days after transplantation. The temporal bones were homogenized in ice-cold lysis buffer. After centrifugation of the homogenized solution, the supernatants were assayed for proteins. The sample solutions were electroblotted onto a polyvinyldifluoride membrane. The primary antibody was a mouse monoclonal anti-FLAG antibody (1:500; Sigma) or rabbit polyclonal anti-β-actin antibody (1:200; Sigma), and the secondary antibody was HRP-conjugated anti-mouse IgG (1:50,000; Amersham Biopharmacia Biotech, Buckinghamshire, UK) or anti-rabbit IgG (1:25,000; Amersham Biopharmacia Biotech). Reactions were visualized by chemiluminescence using an ECL Plus Western blotting reagent pack (Amersham Biopharmacia Biotech).

Measurement of Bdnf levels in the inner ear. To assess the *in vivo* production of Bdnf protein by grafted cells, the inner ears engrafted with NIH3T3/BDNF cells ($n=10$) or NIH3T3/control cells ($n=5$) were removed on day 7 after transplantation. A Bdnf ELISA was performed using the BDNF Emax Immunoassay System (Promega) according to the manufacturer's protocol. All reactions were performed in triplicate. Total protein concentration was measured with the Lowry assay using the Bio-Rad DC Protein Assay (Bio-Rad, Hercules, CA, USA).

Statistical analysis. Results were expressed as means ± standard error. Statistical analyses for Bdnf levels in the cultured medium and ABR threshold shifts were performed using one-way ANOVA followed by Sheffe's multiple-comparison tests. A Mann–Whitney *U* test was used to compare cochlear Bdnf levels. Probability (*P*) values less than 5% were considered significant.

ACKNOWLEDGMENTS

The authors thank Daisuke Yabe and Norio Yamamoto (Department of Medical Chemistry and Molecular Biology, Kyoto University Graduate School of Medicine, Japan) for help and instruction with molecular biology, Junko Okano (Department of Anatomy and Developmental Biology, Kyoto University Graduate School of Medicine) for critical discussion, and Yoko Nishiyama and Rika Sadato for their technical assistance. This study was supported by a Grant-in-Aid for Scientific Research (B2, 16390488, 2004–2006, T.N.) from the Ministry of Education, Culture, Sports, Science, and Technology of Japan and in part by a grant (2005–2006, T.N.) from the Takeda Science Foundation and a grant (2005, T.O.) from the 21st Century COE Program of the Ministry of Education, Culture, Sports, Science, and Technology of Japan.

RECEIVED FOR PUBLICATION MARCH 7, 2006; REVISED JUNE 8, 2006; ACCEPTED JUNE 21, 2006.

APPENDIX A. SUPPLEMENTARY DATA

Supplementary data associated with this article can be found, in the online version, at doi:10.1016/j.ymthe.2006.06.012.

Copyright © The American Society of Gene Therapy

REFERENCES

1. Nance, W. E. (2003). The genetics of deafness. *Ment. Retard. Dev. Disabil. Res. Rev.* **9:** 109–119.
2. Altschuler, R. A., Cho, Y., Ylikoski, J., Pirvola, U., Magal, E., and Miller, J. M. (1999). Rescue and regrowth of sensory nerves following deafferentation by neurotrophic factors. *Ann. N.Y. Acad. Sci.* **884:** 305–311.
3. Gillespie, L. N., Clark, G. M., Bartlett, P. F., and Marzella, P. L. (2003). BDNF-induced survival of auditory neurons in vivo: cessation of treatment leads to accelerated loss of survival effects. *J. Neurosci. Res.* **71:** 785–790.
4. Endo, T., *et al.* (2005). Novel strategy for treatment of inner ears using a biodegradable gel. *Laryngoscope* **115:** 2016–2020.
5. Noushi, F., Richardson, R. T., Hardman, J., Clark, G., and O'Leary, S. (2005). Delivery of neurotrophin-3 to the cochlea using alginate beads. *Otol. Neurotol.* **26:** 528–533.
6. Shinohara, T., *et al.* (2002). Neurotrophic factor intervention restores auditory function in deafened animals. *Proc. Natl. Acad. Sci. USA* **99:** 1657–1660.
7. Kishino, A., *et al.* (2001). Analysis of effects and pharmacokinetics of subcutaneously administered BDNF. *Neuroreport* **12:** 1067–1072.
8. Staecker, H., Gabaizadeh, R., Federoff, H., and Van De Water, T. R. (1998). Brain-derived neurotrophic factor gene therapy prevents spiral ganglion degeneration after hair cell loss. *Otolaryngol. Head Neck Surg.* **119:** 7–13.
9. Chen, X., Frisina, R. D., Bowers, W. J., Frisina, D. R., and Federoff, H. J. (2001). HSV amplicon-mediated neurotrophin-3 expression protects murine spiral ganglion neurons from cisplatin-induced damage. *Mol. Ther.* **3:** 958–963.
10. Yagi, M., Magal, E., Sheng, Z., Ang, K. A., and Raphael, Y. (1999). Hair cell protection from aminoglycoside ototoxicity by adenovirus-mediated overexpression of glial cell line-derived neurotrophic factor. *Hum. Gene Ther.* **10:** 813–823.
11. Hakuba, N., *et al.* (2003). Adenovirus-mediated overexpression of a gene prevents hearing loss and progressive inner hair cell loss after transient cochlear ischemia in gerbils. *Gene Ther.* **10:** 426–433.
12. Nakaizumi, T., Kawamoto, K., Minoda, R., and Raphael, Y. (2004). Adenovirus-mediated expression of brain-derived neurotrophic factor protects spiral ganglion neurons from ototoxic damage. *Audiol. Neurootol.* **9:** 135–143.
13. Stone, I. M., Lurie, D. I., Kelley, M. W., and Poulsen, D. J. (2005). Adeno-associated virus-mediated gene transfer to hair cells and support cells of the murine cochlea. *Mol. Ther.* **11:** 843–848.
14. Cejas, P. J., *et al.* (2000). Lumbar transplant of neurons genetically modified to secrete brain-derived neurotrophic factor attenuates allodynia and hyperalgesia after sciatic nerve constriction. *Pain* **86:** 195–210.
15. Cao, L., *et al.* (2004). Olfactory ensheathing cells genetically modified to secrete GDNF to promote spinal cord repair. *Brain* **127:** 535–549.
16. Girard, C., *et al.* (2005). Grafts of brain-derived neurotrophic factor and neurotrophin 3-transduced primate Schwann cells lead to functional recovery of the demyelinated mouse spinal cord. *J. Neurosci.* **25:** 7924–7933.
17. Iguchi, F., *et al.* (2003). Trophic support of mouse inner ear by neural stem cell transplantation. *Neuroreport* **14:** 77–80.
18. Tateya, I., *et al.* (2003). Fate of neural stem cells grafted into injured inner ears of mice. *Neuroreport* **14:** 1677–1681.
19. Iguchi, F., *et al.* (2004). Surgical techniques for cell transplantation into the mouse cochlea. *Acta Otolaryngol. Suppl.* **551:** 43–47.
20. Kawamoto, K., Oh, S. H., Kanzaki, S., Brown, N., and Raphael, Y. (2001). The functional and structural outcome of inner ear gene transfer via the vestibular and cochlear fluids in mice. *Mol. Ther.* **4:** 575–585.
21. Hildebrand, M. S., *et al.* (2005). Survival of partially differentiated mouse embryonic stem cells in the scala media of the guinea pig cochlea. *J. Assoc. Res. Otolaryngol.* **6:** 341–354.
22. Evans, C. H., *et al.* (2005). Gene transfer to human joints: progress toward a gene therapy of arthritis. *Proc. Natl. Acad. Sci. USA* **102:** 8698–8703.
23. Kakeda, M., *et al.* (2005). Human artificial chromosome (HAC) vector provides long-term therapeutic transgene expression in normal human primary fibroblasts. *Gene Ther.* **12:** 852–856.
24. Naito, Y., *et al.* (2004). Transplantation of bone marrow stromal cells into the cochlea of chinchillas. *Neuroreport* **15:** 1–4.
25. Shiga, A., *et al.* (2005). Aging effects on vestibulo-ocular responses in C57B/6 mice: comparison with alteration in auditory function. *Audiol. Neurootol.* **10:** 97–104.

Copyright © The American Society of Gene Therapy

The Laryngoscope
Lippincott Williams & Wilkins, Inc.
© 2006 The American Laryngological,
Rhinological and Otological Society, Inc.

Cochlear Protection by Local Insulin-Like Growth Factor-1 Application Using Biodegradable Hydrogel

Koji Iwai, MD; Takayuki Nakagawa, MD, PhD; Tsuyoshi Endo, MD; Yoshinori Matsuoka; Tomoko Kita, PhD; Tae-Soo Kim, MD, PhD; Yasuhiko Tabata, PhD; Juichi Ito, MD, PhD

Objective: **The aim of this experimental study was to examine the potential of local recombinant human insulin-like growth factor-1 (rhIGF-1) application through a biodegradable hydrogel for the treatment of cochleae.** ***Methods:*** **A hydrogel immersed with rhIGF-1 was placed on the round window membrane of Sprague-Dawley rats while a hydrogel immersed with physiological saline was applied to control animals. On day 3 after drug application, the animals were exposed to white noise at 120 dB sound pressure level (SPL) for 2 hours. Cochlear function was monitored using measurements of auditory brain stem responses (ABRs) at frequencies of 8, 16, and 32 kHz. The temporal bones were collected 7 or 30 days after noise exposure and the loss of hair cells was quantitatively analyzed.** ***Results:*** **Local rhIGF-1 treatment significantly reduced the elevation of ABR thresholds on days 7 and 30 after noise exposure. Histologic analysis revealed that local rhIGF-1 treatment significantly prohibited the loss of outer hair cells.** ***Conclusions:*** **These findings demonstrate that local IGF-1 application through the biodegradable hydrogel has the potential for protection of cochleae from noise trauma.** ***Key Words:*** **Drug delivery, cochlea, hair cell, protection, growth factor, acoustic trauma, rat.**
Laryngoscope, **116:529–533, 2006**

INTRODUCTION

In recent years, there has been increasing interest in the treatment of inner ear disorders using the local, rather than systemic, application of therapeutic agents, because the former has fewer side effects and is more target-specific. The establishment of clinically applicable strategies for the local application of therapeutic agents should therefore open a new window for the treatment of inner ear disorders. For methods of drug delivery to be viable in clinical settings, it is crucial for the procedure to be technically undemanding and as minimally invasive as possible. Based on such a background, the use of biodegradable polymers for cochlear drug delivery has been investigated.[1–3] Biodegradable polymers, which enable the sustained release of drugs to the cochlear fluid space, can be applied through an intratympanic injection. Among biodegradable polymers, we have reported the efficacy of the biodegradable hydrogel, which is made from porcine type-I collagen, for delivery of brain-derived neurotrophic factor (BDNF) into the cochlear fluid and successful protection of spiral ganglion neurons (SGNs) from degeneration as a result of the loss of cochlear hair cells.[3]

Insulin-like growth factor-1 (IGF-1) is a mitogenic peptide that plays essential roles in the regulation of growth and development in various parts of the body, including the inner ear.[4] IGF-1 is also known to be a neuroprotective agent.[5] In addition, previous studies on the inner ear have suggested the possibility of inner ear protection by IGF-1.[6,7] Moreover, recombinant human IGF-1 (rhIGF-1) has already been approved for clinical use. Our ultimate goal is for local neurotrophin application to be clinically approved for the treatment of inner ears. In the present study, we then selected rhIGF-1 as a suitable neurotrophin for local application to the cochlea using a biodegradable hydrogel as a vehicle for drug delivery. We evaluated whether the application of rhIGF-1 in this manner was effective in protecting against noise-induced hearing loss.

From the Department of Otolaryngology–Head and Neck Surgery (K.I., T.N., T.E., Y.M., T.K., T.-S.K., J.I.), Graduate School of Medicine and the Institute for Frontier Medical Science (Y.T.), Kyoto University, Kyoto, Japan.

Editor's Note: This Manuscript was accepted for publication December 5, 2005.

This study was supported by a Grant-in-Aid for Regenerative Medicine Realization from the Ministry of Education, Science, Sports, Culture and Technology of Japan.

Send Correspondence to Dr. Takayuki Nakagawa, Department of Otolaryngology–Head and Neck Surgery, Graduate School of Medicine, Kyoto University, Kawaharacho 54, Shogoin, Sakyo-ku, 606-8507 Kyoto, Japan. E-mail: tnakagawa@ent.kuhp.kyoto-u.ac.jp

DOI: 10.1097/01.mlg.0000200791.77819.eb

MATERIALS AND METHODS

Experimental Animals

Sprague-Dawley rats (Japan SLC Inc., Hamamatsu, Japan) at 10 weeks of age were used as experimental animals. The Animal Research Committee of the Graduate School of Medicine, Kyoto University, Japan, approved all experimental protocols. Animal care was conducted under the supervision of the Institute of Laboratory Animals at the Graduate School of Medicine, Kyoto University. All experimental procedures were performed in accordance with the U.S. National Institutes of Health guidelines for the care and use of laboratory animals.

Preparation of Hydrogels

The biodegradable hydrogels were prepared as described previously.[8] Briefly, the gels were generated by the glutaraldehyde crosslinking of porcine type-I collagen (Gunze, Ayabe, Japan). The rates of degradation were determined according to the concentration of glutaraldehyde. The present study used a hydrogel that was made with 60 mol/L glutaraldehyde, which could release basic fibroblast growth factor[8] and BDNF[3] for 7 days in vivo.

Local Application of Insulin-Like Growth Factor-1

RhIGF-1 was provided by Astellas Pharma Inc., Tokyo, Japan. After measuring the auditory brain stem responses (ABRs), the otic bulla of the left temporal bone was exposed using a retroauricular approach under general anesthesia with ketamine (100 mg/kg intramuscularly [IM]; Sankyo Co., Tokyo, Japan) and xylazine (9 mg/kg IM; Bayer, Tokyo, Japan). A small hole was made on the left bulla to expose the round window niche. A hydrogel in dry condition was cut into the size of 2 mm^3 under the microscope and immersed with rhIGF-1 (400 μg dissolved in 40 μL physiological saline) 30 minutes before application. The hydrogel was then placed on the round window membrane (RWM) of the IGF group animals (n = 10). The animals applied a hydrogel-immersed physiological saline were used as controls (n = 10).

Noise Exposure and Measurement of Hearing

On day 3 after the IGF-1 application, we measured the ABRs to eliminate animals that showed threshold shifts of more than 10 dB at any frequencies from the experiments. In consequence, no animals showed threshold shifts over 10 dB after local drug application in the present study. The animals were then exposed to white noise at 120 dB sound pressure level (SPL) for 2 hours in a ventilated sound exposure chamber. The sound levels were monitored and calibrated at multiple locations within the sound chamber to ensure uniformity of the stimulus.

Auditory function was assessed by recording ABRs. The measurements of ABR thresholds were performed at frequencies of 8, 16, and 32 kHz before noise exposure and days 7 and 30 after noise exposure. Animals were anesthetized with ketamine (100 mg/kg) and xylazine (9 mg/kg) and kept warm with a heating pad. Generation of acoustic stimuli and subsequent recording of evoked potentials were performed using a PowerLab/4sp (AD Instruments, Castle Hill, Australia). Acoustic stimuli, consisting of tone-burst stimuli (0.1 ms cos^2 rise/fall and 1-ms plateau), were delivered monaurally through a speaker (ES1spc; Bioresearch Center, Nagoya, Japan) connected to a funnel fitted into the external auditory meatus. To record bioelectrical potentials, subdermal stainless steel needle electrodes were inserted at the vertex (ground), ventrolateral to the measured ear (active) and contralateral to the measured ear (reference). Stimuli were calibrated against a ¼-inch free-field microphone (ACO-7016; ACO Pacific, Inc., Belmont, CA) connected to an oscilloscope (DS-8812 DS-538; Iwatsu Electric, Tokyo, Japan) or a sound level meter (LA-5111; Ono Sokki, Yokohama, Japan). The responses between the vertex and mastoid subcutaneous electrodes were amplified with a digital amplifier (MA2; Tucker-Davis Technologies, Alachua, FL). Thresholds were determined from a set of responses at varying intensities with 5-dB SPL intervals and electrical signals were averaged for 1024 repetitions. Thresholds at each frequency were verified at least twice.

Histologic Analysis

On day 7 or 30 after noise exposure, five cochleae from each experimental group were provided for histologic analysis. The animals were anesthetized with ketamine and xylazine, and the left cochleae were exposed. After removal of otic vesicles, 4% paraformaldehyde in 0.01 mol/L phosphate-buffered saline (PBS)

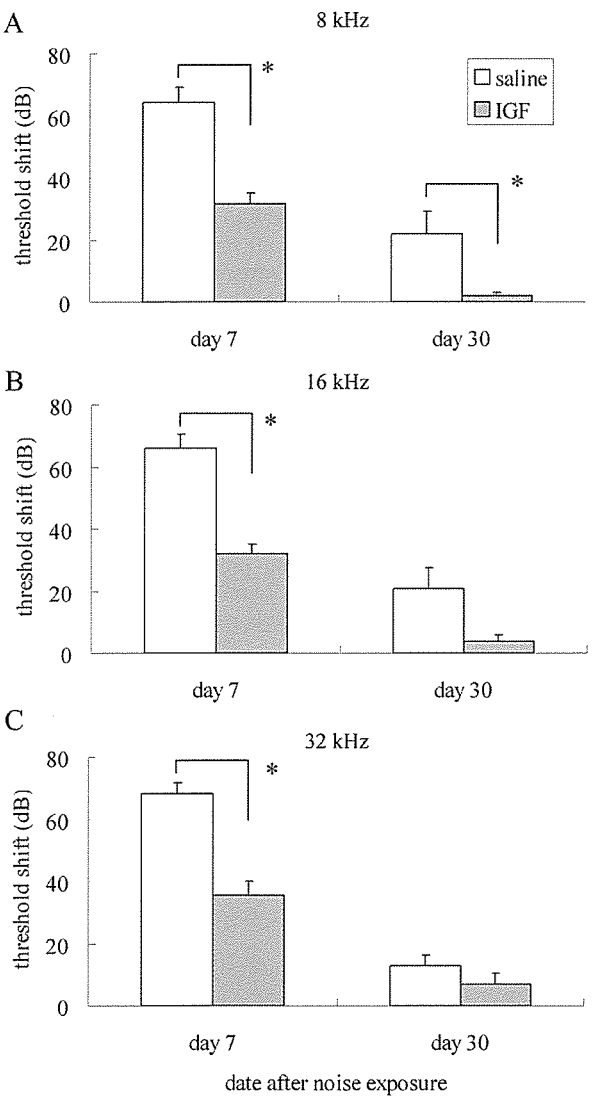

Fig. 1. Auditory brain response threshold shifts for recombinant human insulin-like growth factor-1- (rhIGF-1) and saline-treated cochleae at 8, 16, and 32 kHz on days 7 and 30 after noise exposure. An overall effect of local rhIGF-1 treatment is significant at 8, 16, or 32 kHz (two factorial analysis of variance). Asterisks are indicated significant differences in pairwise comparisons with Fisher's protected least-significant difference. Bars represent standard error (SE).

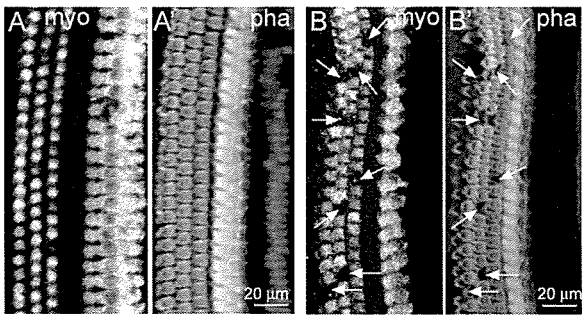

Fig. 2. Photomicrographs of surface preparations stained with myosin VIIa and phalloidin from the second turn of cochleae treated with recombinant human insulin-like growth factor-1 (**A**) or physiological saline (**B**) on day 30. Figures A and B show immunostaining for myosin VIIa (myo), and Figures A' and B' show F-actin labeling by phalloidin. Arrows indicate missing outer hair cells.

at pH 7.4 was gently introduced into the perilymphatic space of the cochleae. The temporal bones were then excised and immersed in the same fixative at 4°C for 12 hours. After rinses with PBS, the cochleae were dissected from the temporal bones and subjected to histologic analysis in whole mounts. We used three regions of cochlear sensory epithelia at a distance of 30% to 40% (apical), 50% to 60% (middle) or 80% to 90% (basal) from the apex for quantitative assessments of hair cell loss.

Immunohistochemistry for myosin VIIa and F-actin labeling by phalloidin were used to label the surviving inner hair cells (IHCs) and outer hair cells (OHCs). Anti-myosin VIIa rabbit polyclonal antibody (1:300; a gift from Tama Hasson, San Diego, CA) was used as the primary antibody, and Alexa-594-conjugated antirabbit goat IgG (1:400; Molecular Probe, Eugene, OR) was used as the secondary antibody. After immunostaining for myosin VIIa, specimens were stained with FITC-conjugated phalloidin (1:300; Molecular Probe). Specimens were viewed using a Leica TCS SP2 confocal microscope (Leica Microsystems Inc., Wetzlar, Germany). Nonspecific labeling was tested by omitting the primary antibody from the staining procedures. We counted the numbers of IHCs and OHCs in 0.2-mm long regions of the apical, middle, or basal portion of cochleae, respectively.

Statistical Analyses

An overall effect on ABR threshold shifts of application of rhIGF-1 was examined by the two-way factorial analysis of variance. When the interaction was significant, multiple comparisons with Fisher's protected least-significant difference (PLSD) were used for pairwise comparisons. The differences in OHC numbers in each region of the cochlea between the rhIGF-1- and saline-treated cochleae were examined using the Student t test. A P value less than .05 was considered statistically significant. Values are expressed as the mean ± standard error.

RESULTS

Functional Protection

The time course of alterations in ABR threshold shifts after noise exposure at 8, 16, or 32 kHz is shown in Figure 1. Local rhIGF-1 treatment demonstrated significant effects on ABR threshold shifts at each frequency. An overall effect on data for 8 kHz of rhIGF-1 application was significant ($P < .001$). The differences in threshold shifts between rhIGF-1- and saline-treated cochleae on days 7 and 30 were significant at multiple comparisons with Fisher's PLSD ($P < .001$ for day 7, $P = .039$ for day 30). An overall effect on data for 16 or 32 kHz of rhIGF-1 application was significant ($P < .001$ for 16 kHz, $P = .005$ for 32 kHz). The difference in threshold shifts at 16 kHz between rhIGF-1- and saline-treated cochleae was significant on day 7 ($P < .001$), but not on day 30 ($P = .051$). The difference in threshold shifts at 32 kHz between rhIGF-1- and saline-treated cochleae was significant on day 7 ($P < .001$), but not on day 30 ($P = .48$).

Histologic Protection

Immunostaining for myosin VIIa and phalloidin staining demonstrated degeneration of OHCs in the apical, middle, and basal portions of saline-treated cochleae (Fig. 2B), whereas OHC degeneration was very limited in rhIGF-1-treated cochleae (Fig. 2A). Conversely, IHC loss was not apparent in every region of both saline- and rhIGF-1-treated cochleae. Quantitative assessments revealed the significant differences in the degree of OHC loss between saline- and rhIGF-1-treated cochleae on days 7 and 30 (Fig. 3). The differences in the degree of OHC loss between the saline- and rhIGF-1-treated cochleae were significant in the apical ($P = .0006$), middle ($P < .0001$), and basal portion ($P = <.0001$) of cochleae on day 7, and in the apical ($P = .0006$), middle ($P < .0001$), and basal portion ($P = .002$) of cochleae on day 30. IHC loss was 2.7 ± 1.3% in the basal, 1.0 ± 0.5% in the middle, or 1.1 ± 0.8 in the apical portion of saline-treated cochleae, and 2.0 ±

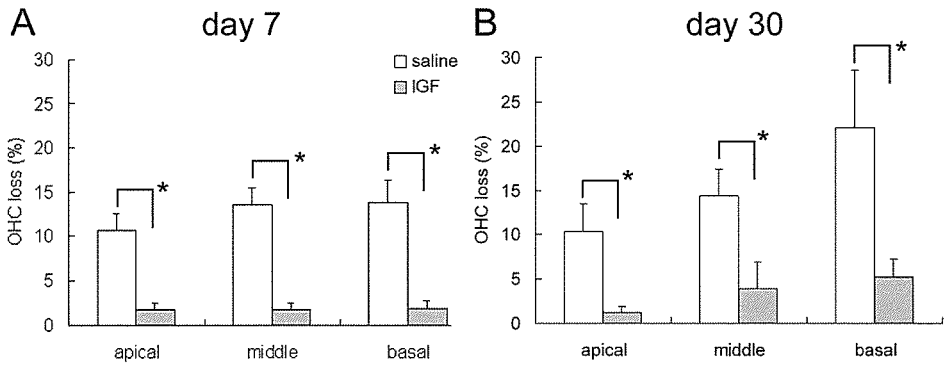

Fig. 3. Means of the percentage outer hair cell loss in the apical, middle, and basal portions of insulin-like growth factor-1- and saline-treated cochleae on days 7 (**A**) and 30 (**B**). Asterisks indicate significant differences with unpaired t test. Bars represent standard error (SE).

1.4% in the basal, 1.2 ± 0.9% in the middle, or 0.6 ± 0.6 in the apical portion of rhIGF-1-treated cochleae on day 30. No significant differences in the loss of IHCs were identified between the two experimental groups.

DISCUSSION

Our findings demonstrate that local rhIGF-1 application using a hydrogel before noise exposure has significant effects on reduction of ABR threshold shifts and of OHC loss. Our previous study has demonstrated the efficacy of local BDNF delivery to the cochlea by the biodegradable hydrogel.[3] The present findings therefore indicate that the biodegradable hydrogel can be used for local rhIGF-1 application to the cochlea. Our previous findings[3] demonstrate that high concentrations of BDNF in the cochlear fluid are maintained during days 3 to 7 after local BDNF application using this system. We then locally applied rhIGF-1 3 days before noise exposure to obtain sufficient concentrations of rhIGF-1 in the cochlear fluid. As expected, the pretreatment with rhIGF-1 demonstrated sufficient protective effects against noise trauma in the present study. However, in clinical settings, drug application after the onset of hearing loss is usually performed. Hence, we should examine the efficacy of local rhIGF-1 treatment after onset of hearing loss in the near future.

In the present study, we focused on degeneration of sensory hair cells in histologic analysis, because the degree of hair cell loss has traditionally been used to evaluate both the extent of noise-induced injury and the efficacy of protective treatments.[9,10] Quantitative assessments in the present study demonstrated significant protection of OHCs from noise trauma by local rhIGF-1 treatment. As for mechanisms of OHC protection by rhIGF-1, several possible explanations are aroused. One possible explanation is the rescue of OHCs from apoptosis resulting from noise by rhIGF-1. IGF-1 is known to inhibit apoptosis by downregulating the expression of proapoptotic genes,[11] and apoptosis is involved in OHC degeneration resulting from noise.[12] Another mechanism is the regulation of glucose transporters in OHCs by rhIGF-1. The expression of glucose transporter-5 (GLUT-5) in OHCs and its importance in their function have been reported.[13,14] GLUTs operate in the first step of glucose utilization by promoting the transport of glucose across the plasma membrane.[15] IGF-1 can regulate the expression of GLUT-5, thereby promoting neuronal cell survival.[16] Such mechanisms might be involved in the rhIGF-1-induced protection of OHCs against noise-induced injury. Further studies are required for elucidation of detailed mechanisms for the rhIGF-1-induced protection of OHCs.

ABR threshold shifts observed on day 7 remarkably recovered on day 30, whereas the damage in the organ of Corti moderately progressed until day 30. This indicates that ABR threshold shifts observed on day 7 may be caused not only by the damage in the organ of Corti, but also by reversible damages in other regions of the cochlea. In addition, the damage in the organ of Corti on day 7, 10% to 14% loss of OHCs and limited loss of IHCs, is not compatible with over 60 dB ABR threshold shifts. Recent studies have indicated involvement of damages in the cochlear lateral wall in noise-induced HL.[17] Local rhIGF-1 treatment significantly reduced ABR threshold shifts on day 7. IGF-1 has also effects on promotion of survival of fibloblasts.[18] Therefore, protective effects of IGF-1 on the fibrocytes in the spiral ligament may be involved in mechanisms for significant reduction of ABR threshold shifts on day 7.

CONCLUSION

This report demonstrates the efficacy of local rhIGF-1 application using a biodegradable hydrogel for the protection of cochleae from noise-induced hearing loss. Because the materials used in the present study are suitable for clinical application, the present findings encourage us to conduct further studies for clinical application of local rhIGF-1 treatment using the biodegradable hydrogel. However, the exact mechanisms by which rhIGF-1 acts in the cochlea are presently unclear and require further research. Furthermore, rhIGF-1 was applied before the onset of noise-induced hearing loss in the present study. The ability of rhIGF-1 to ameliorate cochlear damages when applied locally after the onset of hearing loss should therefore be examined in an experimental model in the near future.

Acknowledgments

The authors thank T. Hasson for providing the antibody for myosin VIIa.

BIBLIOGRAPHY

1. Arnold W, Senn P, Hennig M, et al. Novel slow- and fast-type drug release round-window microimplants for local drug application to the cochlea: an experimental study in guinea pigs. *Audiol Neurotol* 2005;10:53–63.
2. Tamura T, Kita T, Nakagawa T, et al. Drug delivery to the cochlea using PLGA nanoparticles. *Laryngoscope* 2005; 115:2000–2005.
3. Endo T, Nakagawa T, Kita T, et al. A novel strategy for treatment of inner ears using a biodegradable gel. *Laryngoscope* 2005;115:2016–2020.
4. Varela-Nieto I, Morales-Garcia JA, Vigil P, et al. Trophic effects of insulin-like growth factor-I (IGF-I) in the inner ear. *Hear Res* 2004;196:19–25.
5. Linseman DA, Phelps RA, Bouchard RJ, et al. Insulin-like growth factor-I blocks Bcl-2 interacting mediator of cell death (Bim) induction and intrinsic death signaling in cerebellar granule neurons. *J Neurosci* 2002;22: 9287–9297.
6. Staecker H, Van De Water TR. Factors controlling hair-cell regeneration/repair in the inner ear. *Curr Opin Neurobiol* 1998;8:480–487.
7. Malgrange B, Rigo JM, Coucke P, et al. Identification of factors that maintain mammalian outer hair cells in adult organ of Corti explants. *Hear Res* 2002;170:48–58.
8. Iwakura A, Fujita M, Kataoka K, et al. Intramyocardial sustained delivery of basic fibroblast growth factor improves angiogenesis and ventricular function in a rat infarct model. *Heart Vessels* 2003;18:93–99.
9. Keithley EM, Ma CL, Ryan AF, et al. GDNF protects the cochlea against noise damage. *Neuroreport* 1998;9: 2183–2187.
10. Shoji F, Miller AL, Mitchell A, et al. Differential protective effects of neurotrophins in the attenuation of noise-induced hearing loss. *Hear Res* 2000;146:132–142.
11. Linseman DA, Phelps RA, Bouchard RJ, et al. Insulin-like growth factor-I blocks Bcl-2 interacting mediator of cell

death (Bim) induction and intrinsic death signaling in cerebellar granule neurons. *J Neurosci* 2002;22: 9287–9297.
12. Pirvola U, Xing-Qun L, Virkkala J, et al. Rescue of hearing, auditory hair cells, and neurons by CEP-1347/KT7515, an inhibitor of c-Jun N-terminal kinase activation. *J Neurosci* 2000;20:43–50.
13. Nakazawa K, Spicer SS, Schulte BA. Postnatal expression of the facilitated glucose transporter, GLUT 5, in gerbil outer hair cells. *Hear Res* 1995;82:93–99.
14. Belyantseva IA, Adler HJ, Curi R, et al. Expression and localization of prestin and the sugar transporter GLUT-5 during development of electromotility in cochlear outer hair cells. *J Neurosci* 2000;20:RC116.
15. Bell GI, Kayano T, Buse JB, et al. Molecular biology of mammalian glucose transporters. *Diabetes Care* 1990;13: 198–208.
16. Asada T, Takakura S, Ogawa T, et al. Overexpression of glucose transporter protein 5 in sciatic nerve of streptozotocin-induced diabetic rats. *Neurosci Lett* 1998; 252:111–114.
17. Hirose K, Liberman MC. Lateral wall histopathology and endocochlear potential in the noise-damaged mouse cochlea. *J Assoc Res Otolaryngol* 2003;4:339–352.
18. Heron-Milhavet L, Karas M, Goldsmith CM, et al. Insulin-like growth factor-I receptor activation rescues UV-damaged cells through a p38 signaling pathway. *J Biol Chem* 2001;276:18185–18192.

P52A-0032 Distribution of GFP expressing cells in the developing inner ear of pHes1- or pHes5-EGFP transgenic mouse

Jun Kojima, Akiko Nishida, Shinji Takahayashi, Junichi Ito
Department of Otolaryngology-Head and Neck Surgery, Graduate School of Medicine, Kyoto University, Japan

Basic helix-loop-helix (bHLH) transcription factors play crucial roles in development of the central and peripheral nervous systems. To visualize expression of Hes1 or Hes5 gene, pHes1- and pHes5-EGFP transgenic (tg) mice were generated (Ohtsuka et al., 2006). In each transgenic mouse, a promoter of Hes1 or Hes5 gene drives enhanced green fluorescent protein (EGFP) gene. In the inner ear, it is suggested that Hes1 or Hes5 regulate cell division and differentiation of sensory and supporting cell progenitors via notch signaling pathway. By use of immunohistochemical technique, we examined distribution of GFP expressing cells in the inner ear of the transgenic mice from embryonic day 10 (E10) to postnatal day 60 (P60). In the pHes1-EGFP tg mouse inner ear, GFP immunoreactive (GFP-IR) cells were detected from E10 to P60. In the pHes5-EGFP tg mouse inner ear, GFP-IR cells were observed from E16.5 to P15. GFP-IR cells in pHes1-GFP tg mouse are candidates of sensory cell progenitors in mammalian inner ear.

Reference

Ohtsuka et al., 2006. Mol. Cell Neurosci.

P52A-0033 Expression of zfh-5 in the developing mouse brain: mRNA, antisense RNA and protein expression

Yuriko Komine[1], Kenji Nakamura[2], Motoya Katsuki[1], Tetsuo Yamamori[1]
[1]National Institute for Basic Biology, Okazaki, Japan; [2]Mitsubishi Kagaku Institute of Life Sciences, Machida, Japan

ZFH-5 is a transcription factor containing three homeodomains and 19 Zn fingers and expressed in differentiating neurons. We have reported that the level of *zfh-5* mRNA is negatively regulated by antisense transcripts of the *zfh-5* gene. In several types of neurons, including pyramidal cells in the hippocampus and granule cells in the cerebellum, the *zfh-5* antisense RNA is expressed prior to the mRNA; as the level of the antisense RNA gradually decreases, *zfh-5* mRNA starts to be expressed. Recently, we have raised an antibody against mouse ZFH-5 and examined the expression profile of the ZFH-5 protein. In the most regions of the brain, the protein expression pattern contained with that of mRNA. However, in the several types neurons mentioned above, ZFH-5 protein was not detected even when the *zfh-5* mRNA was already expressed. This observation together with other data suggested that the ZFH-5 protein level is regulated by several mechanisms including suppression by the antisense RNA and translational control.

P52A-0034 Zic1 and Zic3 synergetically control forebrain development

Takashi Inoue[1], Maya Ota[1], Kazuhiko Mikoshiba[2], Jun Aruga[1]
[1]Laboratory for Comparative Neurogenesis, RIKEN BSI, Saitama, Japan; [2]Laboratory for Developmental Neurobiology, RIKEN BSI, Saitama, Japan

Zic family zinc finger proteins play various roles in animal development. In mice, five Zic genes (Zic1–5) have been reported. Despite their partially overlapping expression profiles, mouse mutants for each Zic gene show distinct phenotypes, suggesting the functional redundancy of Zic proteins. It is expected that the common and specific roles of mouse Zic proteins can be clarified by studying compound mutant mice. In the present study, we characterized Zic1/Zic3 compound mutant mice. Mice carrying homozygous Zic1 mutant allele together with Zic3 null allele showed defects in midline structures, including abnormalities in forebrain and thalamus. Especially, the compound mutants showed severe anatomical abnormalities in the dorsal and ventral telencephalon and olfactory system, which are not obvious in either Zic1- or Zic3-single mutant. These observations indicate that Zic1, in cooperation with Zic3, have an essential role in controlling proliferation and differentiation of the neuronal progenitors in the medial telencephalon.

P52A-0035 Expression of RP58, a novel zinc finger transcriptional repressor, in developing mouse brain

Chiaki Maruyama, Haruo Okado
Department of Molecular Physiology, Tokyo Metropolitan Institute for Neuroscience, Japan

RP58, a novel zinc finger protein containing a POZ domain, functions as a sequence specific transcriptional repressor. RP58 gene disrupted mice show severe abnormalities in brain cortical layer formation, suggesting that RP58 has a crucial role in cerebral development. To understand the role of this protein in brain development, we examined RP58 gene expression in mouse embryo and adult brain by in situ hybridization. As a result, we found that RP58 transcripts are first detected at embryonic day 10 in the neuroepithelium of the spinal cord and telencephalic vesicle. In the day 13–13 embryos, RP58 transcripts are predominantly observed in the proliferative region but not in outside the nervous system. At E15, RP58 transcripts were detected throughout the neocortex and hippocampus, but not in the thalamus and striatum. In the cortex, the transcripts were detected primarily in cortical neurons, but not in the marginal zones and ventricular zone. In adult mice, RP58 is expressed in neocortical and hippocampal neurons and granule cells in the cerebellar cortex.

P52A-0036 Lack of NZF-2/MyT-1 and NZF-3 transcription factors result in defects of neuronal differentiation and arthrogryposis multiplex congenita

Toshiki Kameyama, Fumio Matsuzaka, Yuzo Kadowawa, Ichiro Maruyoshi
Division of Cell Biology, Fujita Health University, Toyoake, Japan

Neural zinc finger (NZF) proteins are transcription factors with DNA-binding domains of C2HC-type zinc finger motifs. Using P19 cells, we demonstrated that NZFs were expressed transiently during neuronal differentiation, and forced expression of NZF cDNAs resulted in neuronal differentiation. These results suggest that NZF family have a function regulate neuronal differentiation. To elucidate in vivo functions of NZF family in detail, we generate knockout mice of NZF-2 and NZF-3 respectively. NZF-2 null mice are born alive, but die within 10 min after birth with cyanosis. On the other hand, NZF-3 null mice are viable, fertile and appear normal. These mice look normal morphologically. Then we generate double knockout mice of NZF-2 and NZF-3 by intercrossing. Double knockout mice have a feeding problem, abnormalities like arthrogryposis multiplex congenita. And we find out that the spinal nerves projecting forelimb and trunk are decrease dramatically in the double knockout mice embryo.

Available online at www.sciencedirect.com
SCIENCE DIRECT®
Experimental Neurology 198 (2006) 12–24
Experimental Neurology
www.elsevier.com/locate/yexnr

Cell transplantation to the auditory nerve and cochlear duct

Tetsuji Sekiya [a,*], Ken Kojima [a,b], Masahiro Matsumoto [a], Tae-Soo Kim [a], Tetsuya Tamura [a], Juichi Ito [a]

[a] *Department of Otolaryngology—Head and Neck Surgery, Kyoto University Graduate School of Medicine, Sakyo-ku, Kyoto 606-8507, Japan*
[b] *Establishment of International Center of Excellence (COE) for Integration of Transplantation Therapy and Regenerative Medicine, Kyoto University Graduate School of Medicine, Kyoto 606-8507, Japan*

Received 31 May 2005; revised 22 October 2005; accepted 4 November 2005
Available online 22 December 2005

Abstract

We have developed a technique to deliver cells to the inner ear without injuring the membranes that seal the endolymphatic and perilymphatic chambers. The integrity of these membranes is essential for normal hearing, and the technique should significantly reduce surgical trauma during cell transplantation. Embryonic stem cells transplanted at the internal auditory meatal portion of an atrophic auditory nerve migrated extensively along it. Four–five weeks after transplantation, the cells were found not only throughout the auditory nerve, but also in Rosenthal's canal and the scala media, the most distal portion of the auditory nervous system where the hair cells reside. Migration of the transplanted cells was more extensive following damage to the auditory nerve. In the undamaged nerve, migration was more limited, but the cells showed more signs of neuronal differentiation. This highlights an important balance between tissue damage and the potential for repair.
© 2005 Elsevier Inc. All rights reserved.

Keywords: Auditory nerve; Cell migration; Cell transplantation; Embryonic stem cell; Membranous labyrinth; Spiral ganglion cell

Introduction

Cell transplantation provides a potential method to replace the irreversible loss of auditory hair cells and neurons that accompanies many forms of permanent hearing loss. A fundamental requisite is to deliver the potentially restorative cells to the target, usually the site of the lesion, with minimal trauma to the homeostasis of the host. This is particularly difficult in the inner ear because it has a highly specialized and complex anatomy (Fig. 1). Hair cells are an important target for cell replacement, but they occupy a critical position at the boundary between the cochlear chambers that enclose the endolymph and perilymph. The differential ionic composition of these fluids is essential for maintenance of the endocochlear potential that provides the driving force for sound transduction.

Current surgical techniques in the cochlea break the membranes between the chambers, a process that may disturb or, at worst, abolish the residual hearing of the affected patients. This issue applies not only to cell transplantation (Bianchi and Raz, 2004; Brown et al., 1993; Holley, 2002; Ito et al., 2001; Izumikawa et al., 2005; Staecker et al., 2001) (Figs. 1, [1, 1′]–[3]) but also to the inoculation of vectors used for gene transfection (Bianchi and Raz, 2004; Izumikawa et al., 2005) (Fig. 1, [1]). One alternative is to deliver materials into the endolymphatic space through the vestibular aqueduct (Fig. 1, [1′]). However, these procedures may potentially put endolymphatic structures at risk of injury. Another problem with this technique is that the injected materials may enter not only the cochlear but also the vestibular portion of the membranous labyrinth (Fig. 1).

An osmotic pump can be used to deliver various materials such as cells, viral vectors, or pharmacological agents into the perilymphatic space (Brown et al., 1993) (Fig. 1, [2]). Although direct damage to the endolymphatic structures may be attenuated with this technique, this approach may not be totally free from hearing loss due to perilymphatic fluid fistula (Minor, 2003). Another potential danger of one perilymphatic injection technique is that the injected materials could enter the cochlear aqueduct (Fig. 1, CA) and travel through cerebrospinal fluid to the contralateral ear where they could cause unintended effects. More indirectly, the round window niche has been used as the

* Corresponding author. Fax: +81 75 751 7225.
E-mail address: tsekiya@ent.kuhp.kyoto-u.ac.jp (T. Sekiya).

0014-4886/$ - see front matter © 2005 Elsevier Inc. All rights reserved.
doi:10.1016/j.expneurol.2005.11.006

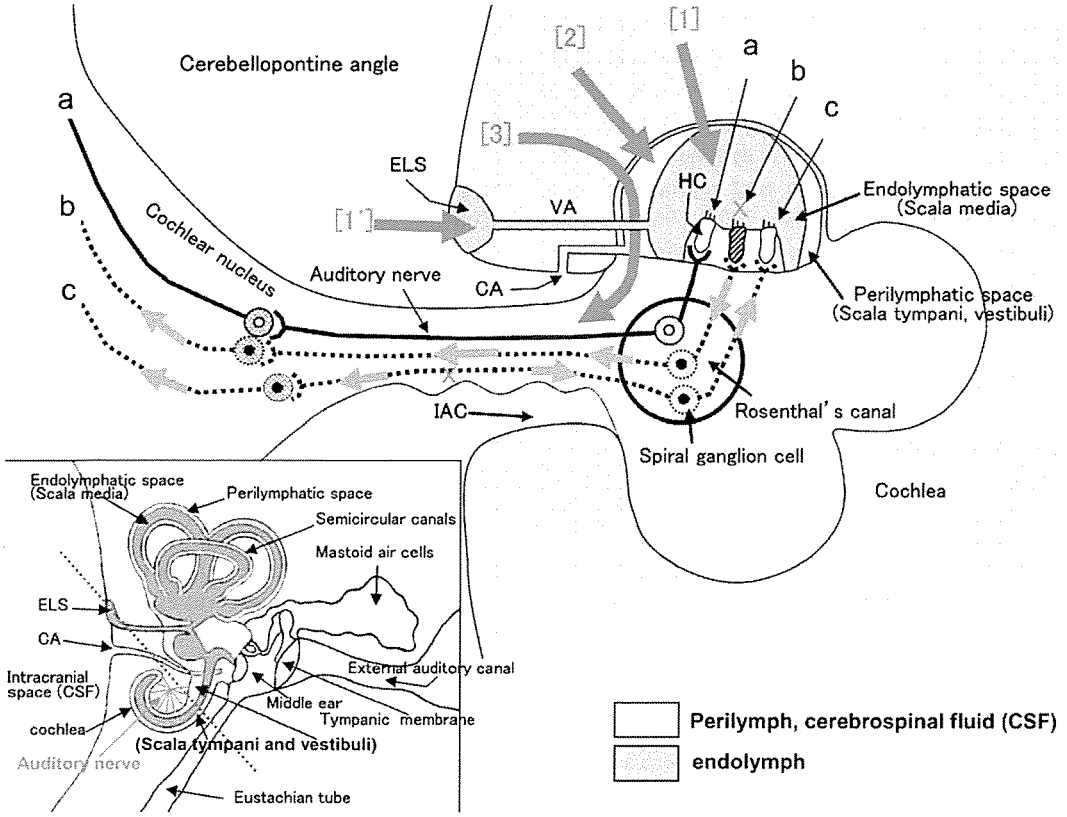

Fig. 1. Schematic representation of normal (a) and pathological (b, c) auditory nerve functional pathways and previously reported approaches ([1], [1′], [2], [3]) to transplanting cells or neuro-regenerative substances into the membranous labyrinth. Normally (a), bipolar auditory neurons synapse with hair cells (HC) distally and with cochlear nucleus cells proximally. When HCs are damaged (b, red x and crosshatched hair cell), degeneration proceeds toward the spiral ganglion neurons and cochlear nucleus cells (b, green arrows). When the auditory nerve is damaged (c) in the CP angle (red x in the middle of the figure), nerve degeneration proceeds bi-directionally as indicated by the green arrows on either side of the x along pathway c. When the membranes enclosing an endo- or perilymphatic fluid-filled space are mechanically breached (interventions [1], [1′], [2], [3]), hearing is compromised. CA, cochlear aqueduct; ELS, endolymphatic sac; IAC, internal auditory canal; VA, vestibular aqueduct. Inset: three-dimensional representation of temporal bone. The blue dotted line indicates the plane of the main figure.

placement site for diffusible materials. However, diffusion of the materials is limited to the more basal turns of the cochlea in this technique, and doses of drugs infiltrating the perilymphatic space are impractical to evaluate. Moreover, non-diffusible materials such as cells cannot be transferred into the membranous labyrinth with this technique.

Transplantation into the modiolus or auditory nerve trunk invades the membranous labyrinth, thus also placing hearing at the risk (Fig. 1, [3]) (Hu et al., 2004a; Regala et al., 2005).

We have developed an effective rat model for cell transplantation in which we have aimed to minimize the damage to cochlear function and potentially to maximize the beneficial outcome. Our method involves transplantation to the internal auditory meatal (IAM) portion of the auditory nerve. To test our model, we transplanted embryonic stem (ES) cells into both damaged and undamaged nerve tissue. We found that transplanted cells migrated along the entire course of the atrophic auditory nerve, even into Rosenthal's canal (RC), where the spiral ganglion cells (auditory ganglion cells) had been located, and finally to the most distal region of the auditory nervous system, the scala media. The fact that cells reached the normal location of the hair cells means that the technique is potentially valuable for replacement of both hair cells and sensory nerves without disrupting the normal balance of endolymph and perilymph. We also found that migration was reduced and neuronal differentiation enhanced in the absence of damage to the nerve. Our technique is based on that refined by the first author over the past 20 years of research in auditory nerve degeneration and regeneration employing more than 5000 experimental animals, including dogs, monkeys, baboons, and, more recently, rats (Sekiya et al., 2000, 2003; Yagihashi et al., 2005).

Materials and methods

Under normal conditions of the auditory nerve and cochlea, spiral ganglion neurons synapse with hair cells distally and with the cochlear nucleus cells proximally (Fig. 1, a). However, various disturbances in nerve transmission can occur and have been described clinically. When the hair cells are damaged, for example, in cases of aminoglycoside ototoxity or sound overstimulation, the spiral ganglion neurons degenerate secondarily (Sekiya et al., 2000; Yagihashi et al., 2005) (Fig. 1, b). Another possible cause is primary pathology in the auditory nerve, such as is seen with auditory neuropathy or with direct surgical trauma during removal of a vestibular schwannoma (Sekiya et al., 2000, 2003; Starr et al., 1996). Under such conditions, the disappearance of spiral ganglion neurons is

caused by retrograde degeneration of the auditory nerve (Fig. 1, c). In both pathological conditions, trans-neuronal degeneration may extend to the cochlear nucleus and upper relay nuclei of the auditory nervous system (Morest et al., 1997) (Figs. 1, b, c). The common element in all of these disorders is degeneration of the spiral ganglion neurons. Therefore, we first reproduced this pathological condition in rats (Sekiya et al., 2000, 2003). In this study, in order to induce direct, rapid, and quantifiable primary degeneration of the auditory nerve, we performed auditory nerve compression in the cerebellopontine (CP) angle of the rat.

Compression of the auditory nerve

All the animal experiments were conducted in accordance with the Guidelines for Animal Experiments at Kyoto University. The auditory nerve of the rats was quantitatively compressed in the CP angle without permanent compromise of the blood supply to the cochlea with the aid of intraoperative monitoring of the compound action potentials of the auditory nerve (CAP) as reported elsewhere (Sekiya et al., 2000, 2003). In the present study, however, we revised the experimental procedures in order to shorten the time during which the labyrinthine artery was transiently compressed. Briefly, male Sprague–Dawley rats weighing 500–550 g each were anesthetized by an intraperitoneal injection of ketamine (100 mg/ml; Sankyo Co., Tokyo, Japan) and xylazine (9 mg/ml; Bayer, Tokyo, Japan). After the rat had been fixed in a small animal stereotactic frame (Model 900, David Kopf Instruments, Tujunga, CA, USA), right suboccipital craniectomy was performed with the aid of a surgical microscope, and the 7th and 8th cranial nerve trunks were identified at the IAM (Sekiya et al., 2000, 2003). An L-shaped stainless steel wire (diameter, 200 μm) was used as the compression-recording (CR) electrode. The CR electrode was placed so that it touched the superior edge of the IAM, and then it was shifted laterally by 7 mm so that its tip touched and remained in contact with the bony surface of the IAM as the electrode was advanced. As the CR electrode was advanced, the auditory nerve was gradually compressed between the tip of the CR electrode and the edge of the IAM (Sekiya et al., 2000). The angle of compression was precisely controlled to apply maximal direct pressure on the nerve with minimal pressure on the artery by having the axis of the electrode tilted posteriorly so the end pointed caudally at an angle of 26.8° from the perpendicular. For the advancement of the CR electrode, a micromanipulator driven by a pulse motor (PC-5N, Narishige, Tokyo, Japan) was used. The operation of this pulse motor was automatically controlled by a programmable controller (Sekiya et al., 2000). As the first compression of the auditory nerve, the CR electrode was advanced at the speed of 1 μm/s until the CAP flattened, termed the "flat point". The CR electrode was maintained at the flat point for 100 s. The rats in which the CAP recovered within 60 s after the flat point was reached, while the CR electrode was maintained at the flat-point position, were included in this study. The depth of electrode advancement for the second compression was 400 μm, and the speed of the electrode advancement was 10 μm/s. Sixty seconds after the start of the second advancement, the electrode was withdrawn at 110 μm/s. In our experimental model, therefore, the auditory nerve and labyrinthine artery were simultaneously compressed during the compression procedure to injure the auditory nerve. However, the duration of complete disappearance of CAPs was less than 60 s in each of two compressions. This amount of CAP loss was far below the critical limit that causes irreversible cochlear ischemia (Pujol et al., 1993; Sekiya et al., 2000).

Electrophysiology

Before the surgical procedures and after the rats were anesthetized, brainstem auditory evoked potentials (BAEPs) were recorded in all rats between the base of the earlobe of the operative side (right) and the vertex with the ground electrode at the base of the forelimb. Click stimuli (90 dB sound pressure level) were presented to the right ear at a rate of 9.5 pulses/s through a tube earphone driven by a 100 μs rectangular pulse wave fed by a stimulator, and evoked potentials were amplified with a bandpass of 50 Hz to 3 kHz and were averaged using a processor (Synax 1100, NEC Medical Systems, Tokyo, Japan) with a sampling interval of 20 μs and 500 data points in each recording. The potentials to 100 successive clicks were averaged and stored in a computer (Sekiya et al., 2000). During the first and second compression procedures, the CAPs were recorded between the tip of the CR electrode and the vertex with the ground electrode placed at the base of the forelimb of the rat. For CAP recordings, the potentials from the nerve to 5 successive clicks were averaged and stored in a computer. This rate led to a continuous CAP recording rate of one potential every 2.4 s before the flat point.

SDIA-treated ES cells

The mouse ES cells that we used, G4-2 (generously donated by Dr. Hitoshi Niwa, Riken Center for Developmental Biology, Kobe, Japan), were a subline derived from E14tg2a ES cells, and they express the enhanced green fluorescent protein (EGFP) gene driven by a ubiquitous strong promoter (CAG promoter) (Kawasaki et al., 2000; Sakamoto et al., 2004). Undifferentiated ES cells were maintained on gelatin-coated dishes in Glasgow minimum essential medium (GMEM) (Invitrogen, Carlsbad, CA, USA) supplemented with 1% fetal calf serum (FCS) (JRH Bioscience, Lenexa, KS, USA), 10% knockout serum replacement (KSR, Invitrogen), 1 mM pyruvate (Sigma, St. Louis, MO, USA), 0.1 mM nonessential amino acids (Invitrogen), 0.2 mM 2-mercaptoethanol (2-ME) (Wako, Osaka, Japan), and 2000 U/ml leukemia inhibitory factor (LIF) (Chemicon, Temecula, CA, USA) for 1 week. Then, the SDIA (stromal-cell-derived inducing activity) method was employed for cell differentiation. Briefly, ES cells were cultured to form differentiated colonies on the PA6 (obtained from RIKEN Cell Bank, RCB1127; a stromal cell line derived from newborn mouse calvaria) feeder layer in GMEM supplemented with 5% KSR, 1 mM pyruvate, 0.1 mM nonessential amino acids, and 0.2 mM 2-ME (differentiation medium) (Kawasaki et al., 2000). The day on which ES cells were seeded on the PA6 feeder layer was defined

as day 0, and, on day 6, ES cell colonies were detached en bloc from the PA6 layer using Collagenase B (Roche Diagnostics, Tokyo, Japan). SDIA-treated ES cells were trypsinized to dissociate into single cells and resuspended in medium at 1×10^5 cells/μl. In the ES cell differentiation method used in the present study, an SDIA promotes neural differentiation of mouse ES cells in vitro before transplantation (Kawasaki et al., 2000).

Transplantation of ES-SDIA cells

Four weeks after compression, we confirmed lack of function of the auditory nerve electrophysiologically by evaluating the results of recordings of BAEPs. Then, the rats were divided into two experimental groups. In the first experimental group (group 1, $n = 9$), we re-anesthetized rats, re-opened the same craniectomy site, and placed enhanced green fluorescent protein (EGFP)-expressing embryonic stem (ES) cells treated with the stromal cell derived inducing activity (SDIA) (labeled ES-SDIA cells) (Kawasaki et al., 2000) at the previously compressed portion (IAM portion) of the auditory nerve. Before placing the cells at the compressed portion of the nerve, we incised the connective tissue capsule of the auditory nerve trunk at the IAM portion in order to facilitate adequate contact between transplanted cells and atrophic auditory nerve fibers. We used utmost caution to avoid additional trauma to atrophic nerve fibers.

In rats in the second experimental group (group 2, $n = 3$), after exposing the auditory nerve as just described, the fused silica tube was inserted into the auditory nerve trunk and then was advanced toward the fundus of the IAC approximately 500 μm. We then infused 5-μl portions of ES cell suspension (1×10^5 cell/μl) in phosphate-buffered saline (PBS), using a microinjector (Micro4, World Precision Instruments, Sarasota, FL, USA), over a period of 5 min.

The external and internal diameters of the fused silica tube for peri-neural transplantation (Group 1) were 170 and 100 μm, while those for intra-auditory nerve transplantation (Group 2) were 107 and 40 μm, respectively.

In both groups of rats, when the tube was in place, we covered the transplantation site with a small piece of absorbable gelatin sponge (Spongel, Yamanouchi, Tokyo, Japan) followed by fibrin glue (Beriplast P, ZLB Behring) to prevent spillage of transplanted cells. No immunosuppressant drugs were employed in the present study.

In order to identify differences in the biological behavior of cells transplanted into normal or atrophic nerve, we transplanted the same volume of the same cells to the IAM portion of an intact auditory nerve ($n = 3$), using the same technique used in group 1 rats.

After the cell transplantation procedure, the rats were kept alive for 4–5 weeks. Then, the animals were killed, and the temporal bones were prepared for histological study.

Another 4 rats were killed 4 weeks after compression without cell transplantation in order to investigate the functional and morphological states of the auditory nerve and cochlea after compression.

Immunohistochemistry

Four to five weeks after cell transplantation, each rat was placed in a state of deep anesthesia and was perfused transaortically with 4% paraformaldehyde in 0.01 M phosphate-buffered saline (PBS) at pH 7.4. Three hours later, both temporal bones and the brain stem were removed en bloc. The tympanic bulla was opened, and the specimen was then immersed in the same fixative for 30 min at 4°C, after which both temporal bones were removed and decalcified with 10% ethylenediaminetetraacetic acid (EDTA) and HCl solution (pH 7.4) for 7 days at 4°C. Serial 5 μm frozen sections of each temporal bone embedded in OCT compound (Sakura Finetechnical, Tokyo, Japan) were made. Among the slices made from these procedures, the section that simultaneously included all four RCs (basal, lower middle, upper middle, and apical) as large as possible and the cochlear nerve with widest width possible was selected as midmodiolar sections. The midmodiolar sections were mounted on glass slides, washed in PBS, and dried in room temperature (RT) air for 30 min. The sections were permeabilized and blocked by 10% goat serum in 0.2% Triton X-100 (Sigma) in PBS at RT for 30 min. A primary antibody (anti-EGFP rabbit serum, ×500; Molecular Probes, Tokyo, Japan, diluted by 10% goat serum in 0.2% Triton X-100 PBS) was applied to the sections and incubated at 4°C for 12 h followed by washing in 0.2% Triton X-100 PBS 2 times for 5 min each. A secondary antibody (Alexa Fluor 594 labeled anti-rabbit IgG goat antibody ×500, Molecular Probes, diluted by 10% goat serum in 0.2% Triton X-100 PBS) was applied to the sections at 4°C for 6 h followed by washing in 0.2% Triton X-100/PBS 2 times for 5 min each. For nuclear staining, the sections were incubated in 4′-diamidino-2-phenylindole (DAPI) (0.1 μg/ml, Roche Molecular Biochemicals, Tokyo, Japan) solution at RT for 30 min. In several sections, nucleic acid dye (TOTO3, ×500, Molecular Probes) was applied for 15 min to stain nuclei for confocal microscopy. They were washed in 0.2% Triton/PBS 2 times for 5 min each. The sections were pre-equilibrated in the SlowFade Equilibration Buffer (Molecular Probes) for 30 min and mounted in SlowFade antifade reagent (Molecular Probes). In several rats, anti-βIII-tubulin rabbit polyclonal antibody (×300; Covance Research Product, Berkeley, CA, USA) was used as the primary antibody to visualize neurites. In each case, the non-operated sides of the cochlea and auditory nerve were used as the control. A fluorescence microscope system equipped with appropriate filters (Olympus BX50 + BX-FLA, Olympus, Tokyo, Japan) was used for observation. Samples were photographed with a digital camera (Olympus DP10). For confocal microscopy, a Leica TCS SP2 confocal laser-scanning microscope (Leica Microsystems, Tokyo, Japan) was used. Images used for the figures were processed with Photoshop and Illustrator software programs (Adobe Systems, Mountain View, CA).

We also performed immunohistochemistry to convert the EGFP into the horseradish peroxidase (HRP) reaction to reconfirm the presence of transplanted EGFP-labeled cells in selected cases. After inactivating endogenous peroxidase with 3% hydrogen peroxide, the sections were permeabilized with

0.1% Triton X-100 (Sigma) in PBS and immunoblocked with 10% goat serum in 0.2% Triton X-100 PBS. A primary antibody for EGFP (anti-EGFP rabbit serum, ×500; Molecular Probes, diluted by 10% goat serum in 0.2% Triton X-100 PBS) was applied to the sections at 4°C for 12 h followed by washing in 0.2% Triton X-100 PBS 2 times for 5 min each. Next, the sections were incubated in Histofine Simple Stain Rat MAX-PO (Multi) (Nichirei, Tokyo, Japan) at RT for 30 min. After washing them in 0.2% Triton X-100 PBS 2 times for 5 min each, color was developed with DAB (3,3′-diaminobenzidene) solution using DAB substrate kit (Vector Laboratories, Burlingame, CA, USA) at RT for 10 min. Then, the sections were washed in distilled water (DW) on rotator 2 times for 5 min each. The nuclei were stained with Hematoxylin solution (Wako, Osaka, Japan) for 1 min. The sections were dehydrated in a concentration-ascending alcohol series, fixed with xylene and mounted on slides using Mount in Entellan R neu (Merk, Darmstadt, Germany) and viewed under a light microscope (Olympus BX50, Tokyo, Japan).

Surface preparation analyses

Immunofluorescence analyses were performed on whole-mount surface preparations of cochleae from 4 rats that had undergone auditory nerve compression without cell transplantation. Each animal was placed under deep anesthesia and then perfused intracardially with 0.01 M phosphate-buffered saline (PBS) followed by 4% paraformaldehyde in PBS. The temporal bones were then collected and immersed in the same fixative for 4 h at 4°C. After decalcification, cochleae were microdissected for surface preparation. After rinses with PBS, the samples were permeabilized and blocked by 10% goat serum in 0.2% Triton X-100 PBS at RT for 30 min. The samples were then incubated overnight at 4°C with anti-myosin VIIa polyclonal rabbit IgG antibody (×500; purchased from Tama Hasson, University of California, San Diego, CA, USA) to detect hair cells. After washing in 0.2% Triton X-100 PBS 2 times for 5 min, the samples were incubated for 1 h at RT with goat anti-rabbit IgG-Alexa 546 conjugated (×200 dilution; Molecular Probes). After rinsing on PBS, the samples were mounted onto glass slides, coverslipped with Vectashield mounting medium (Vector Laboratories), and viewed with a confocal laser-scanning microscope (TCS-SP2 Leica Microsystems, Tokyo, Japan).

Results

Compression of the internal meatal portion of auditory nerve causes loss of spiral ganglion neurons with hair cells spared

In the rats that were killed 4 weeks after compression without transplantation, the BAEPs profoundly deteriorated, with loss of all peaks (Fig. 2A). Histological examination of the temporal bones of these rats revealed profound atrophy of the auditory nerve and spiral ganglion cells in each RC (Fig. 2B). In contrast, it was noted that surface preparation studies revealed the preservation of hair cells. In the basal (the region of 80–100% from the apex) and the middle (the region of 50–70% from the apex) cochlear turns, the number and configuration of hair cells were normal or near-normal, although some disturbances were observed in the apical area (the region of 10–30% from the apex (Fig. 2C)).

Cells transplanted at the IAM portions of atrophic auditory nerves extensively migrate (group 1) (Figs. 3–5)

In rats (group 1) that had undergone auditory nerve compression followed by transplantation of ES-SDIA cells at the IAM portion of the auditory nerve, we found ES-SDIA cells at a total of 32 locations (10 different sites, including the transplantation site) (Figs. 3A, B). We found transplanted cells at the transplantation site in 4 of these 9 rats and at the fundus of the internal auditory canal (IAC) in 5 of the 9 rats (Fig. 3B). In one rat, a substantial number of DAB-positive transplanted cells were found at the fundus of the IAC 32 days after transplantation (Figs. 4A-a, b). Most of the cells at the fundus were round, although some appeared to have short projections (Fig. 4A-b, inset).

Generally, the shape of the transplanted cells varied according to the sites where they were found. In one rat with transplanted cells in various regions of the auditory nerve and cochlea 31 days after transplantation (Figs. 4B-a, b), the transplanted cells in the middle of the auditory nerve trunk were elongated, without processes, and aligned in tandem (Fig. 4B-a, inset). Transplanted cells found at the Schwann–glial junctional zone in this rat had several EGFP-positive neuritic processes extending toward the peripheral myelin portion (Fig. 4B-c).

In one rat, several clumps of DAB-positive cells were found within the endolymphatic space in the scala media (Figs. 5A–C). One of these cell clumps was attached to the habenula perforata (HP) region where auditory nerve fibers emerge from RC into the scala media (Fig. 5C). In this rat, transplanted cells were found in the bony canal (tractus spiralis foraminosus) connecting the modiolus and RC (Fig. 5D). The transplanted cells were observed in the scala media in 3 of the 9 rats tested in this group (Figs. 3, 5).

In 8 of the 9 rats examined, a few transplanted cells were found in the perilymphatic space (Figs. 3, 4B-b).

Transplantation of cells into atrophic auditory nerve trunk, an efficient way to deliver cells into Rosenthal's canal (group 2)

In 2 of the 3 rats that had undergone auditory nerve compression and then transplantation of ES-SDIA cells into the auditory nerve trunk, most transplanted cells were retained within the nerve trunk (Figs. 6A, B). In one of these rats, the transplanted cells appeared as a relatively large cell mass within the auditory nerve trunk 32 days after transplantation (Fig. 6A-a). Confocal microscopy revealed that neurites extended distally from the cell mass, between the Schwann cells (Figs. 6A-b, c, d). In this rat, we found a substantial number of the transplanted cells within RC (Figs. 6A-e, f) and several cell clumps in the scala tympani (Fig. 6A-a). In another rat in this group, a cluster of the ES-SDIA cells was seen within the auditory nerve trunk 35 days after transplantation (Fig. 6B-a), with long neuritic

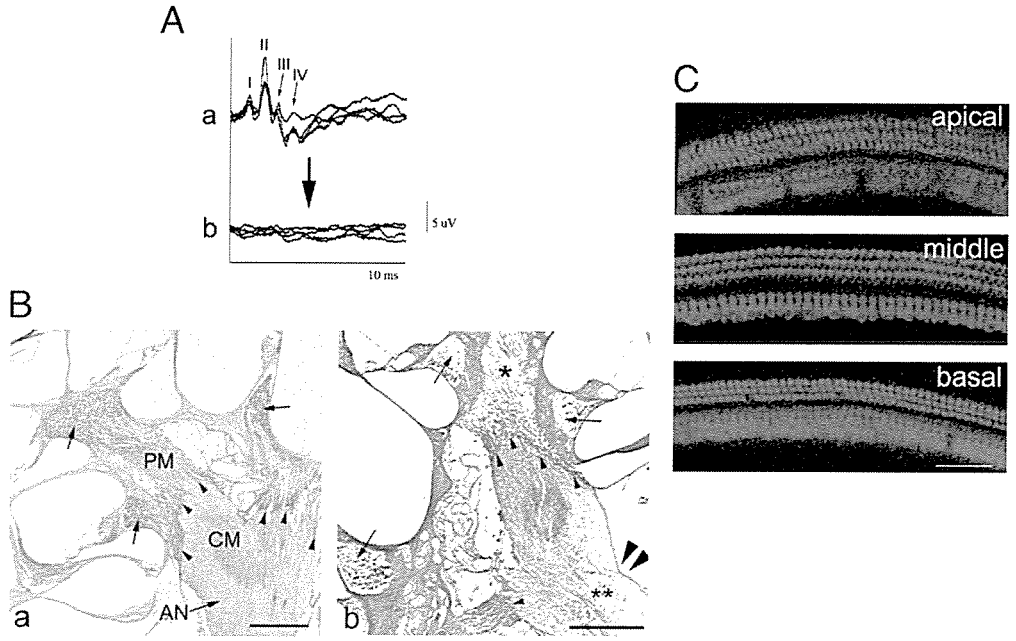

Fig. 2. Auditory nerve degeneration after auditory nerve compression with hair cell spared. (A) Brainstem auditory evoked potentials (BAEPs) before compression (a) and 4 weeks after compression (b). Following compression, all peaks of waves I to IV present before compression (in a) disappeared. (B) Light-microscopic view of the auditory nerve and cochlea in sections from a control (a) and an experimental rat 4 weeks after compression of the auditory nerve (b). Rosenthal's canal in the control rat is densely packed with spiral ganglion cells (arrows in a), but, 4 weeks after compression, the number of spiral ganglion cells in RC of the experimental rat had decreased remarkably (arrows in b) and multiple cavitations were seen (** in b) at the compressed site of the auditory nerve (double arrow heads). A decrease in auditory nerve fibers in the modiolus was seen after compression (* in b). The dome-shaped Schwann–glial junctional zone (SGJ) is indicated by arrow heads. This dome-shaped SGJ is also observed in Figs. 4B and 7. AN, auditory nerve; CM, central myelin portion of the auditory nerve; PM, peripheral myelin portion of the auditory nerve. Hematoxylin–eosin staining. Scale bars, 200 μm. (C) Confocal microscopic views of surface preparations of the cochlea showing the preservation of hair cells. In the basal (the region of 80–100% from the apex) and the middle (the region of 50–70% from the apex) cochlear turns, the number and configuration of hair cells were normal or near-normal. Some disturbances were observed in the apical area (the region of 10–30% from the apex). Scale bars, 50 μm.

processes extending into RC through the bony canals connecting the modiolus and RC (tractus spiralis foraminosus) (Fig. 6B-b).

Cells transplanted to an intact auditory nerve do not migrate

When the same volume of ES-SDIA cells was placed at the IAM portion of an intact auditory nerve, after incision of the connective tissue capsule of the auditory nerve trunk, the results were different from those seen when cells were transplanted to the same location adjacent to an atrophic auditory nerve. In one rat in this group, transplanted cells at the site of transplantation had remarkably extended neurites into the auditory nerve trunk both rostrally and caudally by 32 days after transplantation (Figs. 7A–F), a finding not observed in the rats in group 1 (with atrophic nerves). One neurite that had extended into the peripheral myelin portion of the intact auditory nerve was quite long, and its tip had the shape of a growth cone (Fig. 7B). Although several EGFP-positive cell bodies were observed within the auditory nerve trunk (Fig. 7F), we did not find any transplanted cell bodies very far distant from the site of transplantation.

Discussion

We have demonstrated a technique for cell transplantation to the inner ear that does not involve damage to the membranes that seal the endolymphatic and perilymphatic chambers. Maintenance of the integrity of these chambers is crucial to the auditory system and will significantly reduce the effects of surgical trauma. The technique may have clinical benefits in the future, but it also provides a more controlled model for analysis of the potential for cell transplantation into the inner ear.

We have also demonstrated for the first time that transplanted ES cells can migrate along an atrophic auditory nerve to the scala media where the hair cells reside. The extent of cell migration was related to the compression injury imposed on the auditory nerve. We have yet to demonstrate functional integration of transplanted cells, a challenge that will require further experimentation with a range of different types and preparations of donor cells.

Transplanted cells are transferred to the scala media through atrophic auditory nerve

Successful cell transplantation will depend on how easily transplanted cells can access different parts of the inner ear. The injection site is critical in terms of minimizing tissue damage while placing cells as close as possible to their target site. The migratory behavior of injected cells will determine their ability to locate and replace the target cell populations. The present finding that transplanted cells can travel from the initial grafted site at the IAM portion of the auditory nerve to the most distal end of the auditory nervous system, the scala media where the hair cells reside, suggests a potential delivery route with minimal surgical invasion.

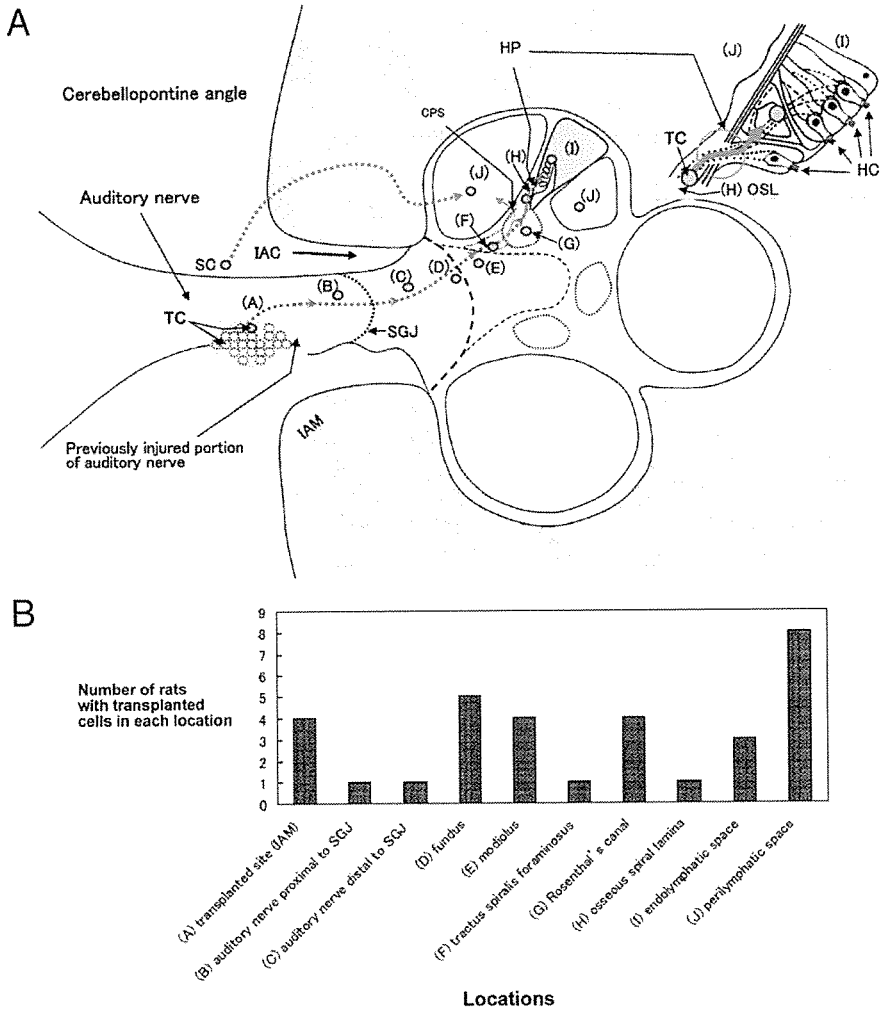

Fig. 3. Cell distribution after transplantation in group 1. (A) Schematic map of the distribution of ES-SDIA cells transplanted at the IAM portion of the auditory nerve (A) in a total of 9 rats. By 4 to 5 weeks after transplantation, the transplanted cells (TC) were found in a total of 32 locations (10 different sites, shown by orange circles) in the 9 rats. The 10 different sites included the transplantation site (A); the auditory nerve proximal (B) and distal (C) to the Schwann–glial junctional zone (SGJ); the fundus of the internal auditory canal (IAC) (D); the modiolus (E); the tractus spiralis foraminosus (F); Rosenthal's canal (G); the osseous spiral lamina (H); the endolymphatic space (I); and the perilymphatic space (J). The blue arrow heads and red solid and dotted arrows indicate the probable route by which the transplanted cells migrated. Spilled cells (SC) probably entered the perilymphatic space (J) through the cochlea aqueduct (Fig. 1, CA) (red dotted curved arrow from SC to (J). CPS, canaliculae perforantes of Schuknecht; HP, habenula perforata. Inset: In the right upper corner is a magnified view of the HP region. HC, hair cells; OSL, osseous spiral lamina. (B) Number of rats (ordinate) with transplanted cells in each of the 10 sites in the auditory nerve and cochlea (abscissa). The sites labeled A to J correspond to those with the same labels in A.

Histopathological examinations of human temporal bones invaded by neoplastic cells indicate that the narrow bony canals between the modiolus and RC (tractus spiralis foraminosus, Figs. 3A–F) serve as a barrier for the passage of cells into RC (Hoshino et al., 1972). In the present study, however, transplanted cells were found within the tractus spiralis foraminosus itself (Figs. 3, 5D) and even in the HP region (Figs. 3, 5C). From these findings, it is likely that transplanted cells reached the scala media by migrating through the HP. Normally, auditory nerve fibers are tightly packed and constricted as they pass through the HP and then they spread out to innervate the hair cells (Spoendlin, 1987). Therefore, under normal conditions, there may be limited space at the HP for the passage of transplanted cells. The apparent ease with which cells migrated along the atrophic nerve could be due to reduced density of the host tissue. Degeneration of the nerve fibers could leave enough space in the HP for transplanted cells to pass through (Fig. 2B-b). The degenerated nerve may produce signals that facilitate cell migration, but we have no evidence for this possibility. In fact, atrophy of the auditory nerve seemed to be required for cell migration because cells transplanted to intact auditory nerves did not migrate so far (Fig. 7). However, space may not be the only influence since undamaged host nerve tissue may restrict migration by direct inhibition or by more effective induction of cell differentiation such as neurite extension. In undamaged nerve tissue, transplanted cells extended numerous neurites into the nerve trunk and remained at the site of transplantation (Figs. 7A, B).

We think it unlikely that the cells we transplanted migrated into the endolymphatic space through the vestibular aqueduct

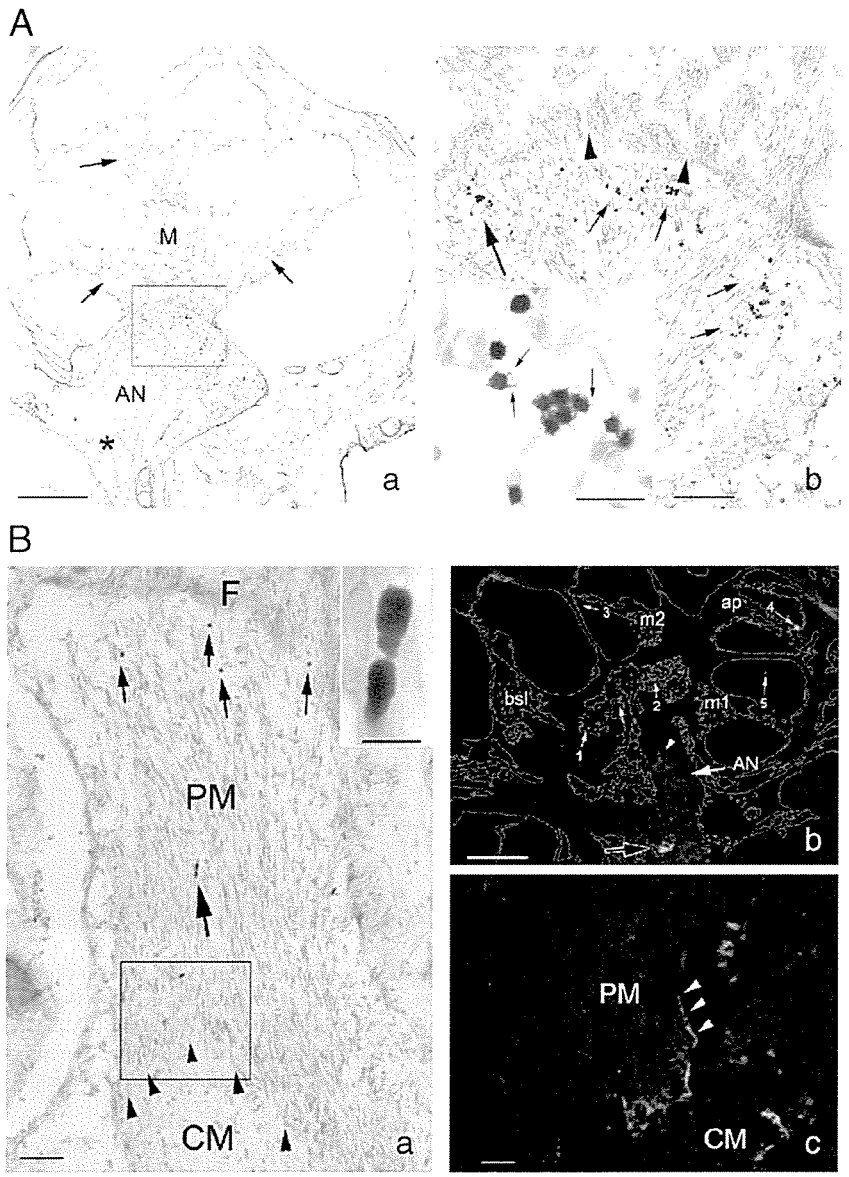

Fig. 4. Migration of ES-SDIA cells transplanted at the IAM portions of atrophic auditory nerves (group 1). (A) Histological appearance of the cochlea showing transplanted ES-SDIA cells accumulated at the fundus of the internal auditory canal in a rat of group 1 (32 days after transplantation). (a) The area of compression and subsequent transplantation of ES-SDIA cells at the auditory nerve (AN) is indicated by the asterisk. The fundus of the internal auditory canal is indicated by the rectangle and enlarged in b. The arrows indicate the Rosenthal's canals. M, modiolus. (b) A substantial number of DAB-positive transplanted cells were found at the fundus (arrows). A group of these cells indicated by the large arrow is enlarged in the inset. In this rat, the transplanted cells were round, and some had short processes projecting from the cell surface (arrows in the inset). The arrow heads indicate the bony holes in the cribriform area that had passed the auditory nerve fibers. Scale bars, 500, 100, and 5; a, b, and inset in b, respectively. (B) Histological appearance of the auditory nerve and cochlea in another rat in group 1 (31 days after transplantation of ES-SDIA cells). (a) DAB-positive transplanted cells (small and large arrows) are present in the auditory nerve trunk. The cells indicated by the large arrow are enlarged in the inset. In this rat, the transplanted cells were elongated, without neuritic processes (inset) and aligned in tandem (compared with findings in A-b). The area indicated by the rectangle is enlarged in c. Arrow heads indicate the dome-shaped Schwann–glial junctional zone. F, fundus of the internal auditory canal. CM and PM, central and peripheral myelin portion of the auditory nerve, respectively. (b) The large black arrow indicates the EGFP-positive cells at the compressed and transplanted portion of the auditory nerve. EGFP-positive cells were observed in various regions such as peri-auditory nerve space (small arrow 1), auditory nerve trunk (2), scala tympani (3), scala media (4), and scala vestibuli (5). An arrow head indicates the area indicated by the rectangle in a. Rosenthal's canal in basal, lower middle, upper middle, and apical cochlear turns are represented by bsl, m1, m2, ap, respectively. (c) At the Schwann–glial junctional zone of this rat, EGFP-positive neuritic process extended toward the peripheral myelin (PM) portion of the auditory nerve (arrow heads). The host auditory nerve stained with DAPI (blue). CM and PM, central and peripheral myelin portion of the auditory nerve, respectively. Scale bars, 500 (5), 20 μm in a (inset), b, c, respectively.

(Fig. 1, [1′]) because the operative site was remote from the aperture of the vestibular aqueduct. In this study, however, transplanted cells were found in the perilymphatic space, mainly in the scala tympani (Figs. 3, 4B-b and 6A-a). It is probable that some transplanted cells entered the cerebrospinal fluid in the CP angle during transplantation and that these cells entered the perilymphatic space through the cochlear aqueduct (Fig. 1, CA). It is also possible that the cells reached the scala tympani by migration from RC through the canaliculae perforantes of Schuknecht (Fig. 3A, CPS). Such coincidental spillage of cells

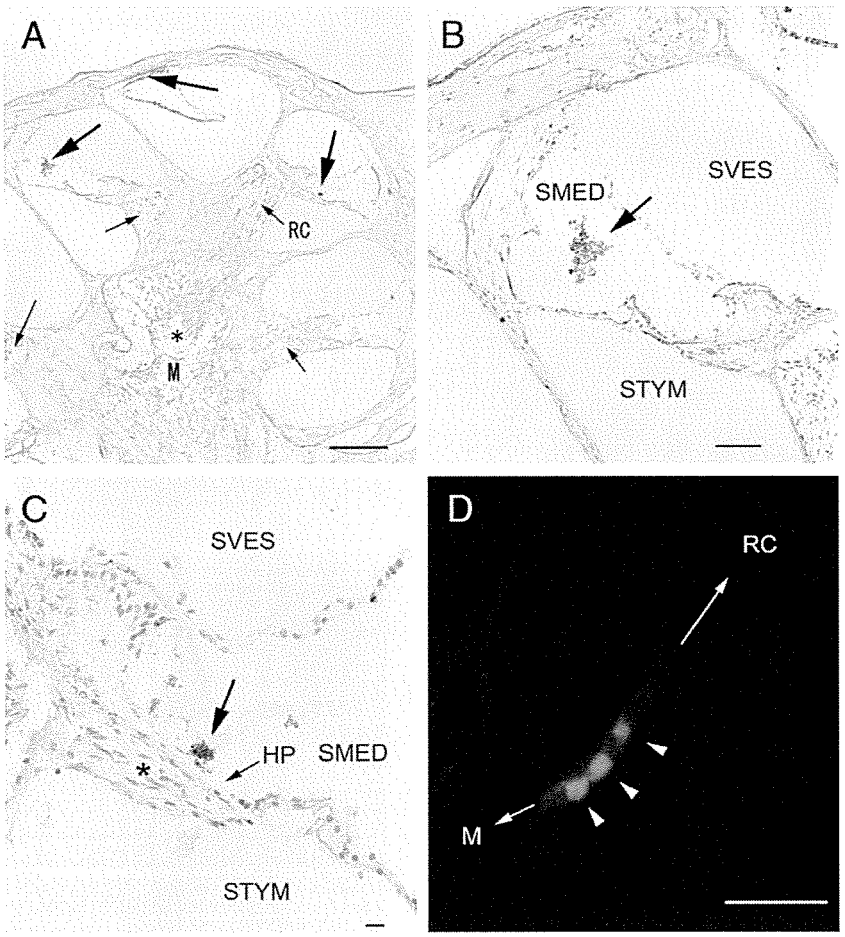

Fig. 5. Migration of ES-SDIA cells transplanted at the IAM portions of atrophic auditory nerves (group 1). (A) Several clumps of DAB-positive cells were found within the endolymphatic space (larger arrows). Two of these cell masses are shown enlarged in B and C. Note empty Rosenthal's canals (RC, small arrows) and paucity of auditory nerve fibers (*) in the modiolus (M). (B) A clump of transplanted cells was found in the scala media (SMED) (arrow). (C) A clump of transplanted cells (arrow) was seen near the habenula perforata (HP) region. Spindle-shaped nuclei of Schwann cells were seen in the osseous spiral lamina (*). (D) EGFP-positive transplanted cells were observed in the bony canal (tractus spiralis foraminosus; arrow heads). The directions to the modiolus and Rosenthal's canal are indicated by M and RC, respectively. Scale bars, 200, 50, 20, and 20 μm in A, B, C, and D, respectively.

may be prevented with future refinements in technique. We found no evidence for substantial accumulation or proliferation of transplanted cells in the perilymphatic space. However, we must be cautious when positioning materials in spaces that communicate with the cerebrospinal fluid space in order to avoid unwanted effects of transplanted materials at inappropriate locations such as the contralateral intact ear.

Local environmental cues and cells with potential for region-specific differentiation

The ES cells we used in this particular study showed a robust migratory ability in the atrophic auditory nerve and were observed at the entire regions of the peripheral auditory nervous system. Ideally, however, the transplanted cells should halt their migration at the target site and then differentiate into region-specific mature cells, for example, spiral ganglion neurons or hair cells. Successful differentiation is likely to depend on local environmental cues and on the capacity of transplanted cells to receive and respond to those cues. In the present study, cells transplanted into the normal auditory nerve extended neuritic processes and expressed βIII-tubulin (Figs. 7B, C, D, F), but their migration was more restricted. This indicates contextual responses to environmental cues and suggests that some degree of morphological integration of the transplanted cells actually occurred. The normal adult tissue could present cues to induce neurite extensions, and it may even restrict unwanted migration, which could be crucial therapeutically. For example, residual nerves in patients with hearing loss could well be essential for attracting transplanted cells into Rosenthal's canal and inducing their differentiation. In the present study, we induced nearly total loss of SGNs in a relatively acute manner (Fig. 2B-b). However, in our experimental model, by regulating the experimental conditions of auditory nerve compression, we can reproduce a similar situation as observed clinically where fewer SGNs gradually degenerate.

The finding that the transplanted cells assumed various shapes according to the sites where they were found implied that they had been influenced by local environmental cues (Fricker et al., 1999; LaBarge and Blau, 2002). The cells at the fundus were round in shape with cell processes (Fig. 4A-b), but those within the nerve tissue assumed a streamlined shape, without cell processes (Fig. 4B-a). An interesting finding of our study